

The ~270 Ma palaeolatitude of Baltica and its significance for Pangea models

Ada R. Dominguez,¹ Rob Van der Voo,¹ Trond H. Torsvik,² Bart W. H. Hendriks,³ Alexandra Abrajevitch,⁴ Mathew Domeier,¹ Bjørn T. Larsen,⁵ and Sonia Rouse⁶

¹Department of Geological Sciences, University of Michigan, Ann Arbor, MI 48109-1005, USA. E-mail: voo@umich.edu

²Physics of Geological Processes, University of Oslo, Postboks 1048 Blindern 0316, Oslo, Norway

³Geological Survey of Norway, PB 3006 Lade, N-7002 Trondheim, Norway

⁴Research School of Earth Sciences, the Australian National University, ACT 0200, Canberra, Australia

⁵Det Norske Ojeselskap, P.O. Box 2070 Vika, 0125 Oslo, Norway

⁶Laboratoire de Mecanismes et Transferts en Geologie, Observatoire Midi-Pyrenees, University of Toulouse, Toulouse, France

Accepted 2011 April 28. Received 2011 April 21; in original form 2010 September 14

SUMMARY

To better constrain Baltica's position within Pangea, we conducted a palaeomagnetic study of Permo-Triassic dykes from the Oslo Graben, as a follow-up to an initial, but rather limited, study by Torsvik and colleagues in 1998. The age of these so-called Lunner dykes had previously been determined as ~240 Ma in that study, but details in their analyses and new ⁴⁰Ar/³⁹Ar ages reveal that there may have been some argon loss in the initially dated dyke minerals and that a combined (weighted mean) age of 271 ± 2.7 (2 σ) Myr for the dykes is preferable. We find two major components of magnetization in our samples: one carried by an Fe-sulphide (likely pyrrhotite) and the other carried by low-Ti magnetite; these magnetization components may be found together (superposed) in a given sample or they may occur apart. Micronmetre-sized crystals of Ti-Fe oxides, observed with a scanning electron microscope (SEM) show exsolution lamellae, formed upon cooling from intrusion temperatures. Assuming that the submicronmetre-sized (Ti)-magnetite grains that carry a stable remanence are of the same generation as the observed larger grains, we interpret the magnetite remanence in the dykes as of primary, thermoremanent origin. The sulphide remanence appears to be slightly younger, as seen by the SEM observations of pyrite framboids and a Fe-sulphide grain invading a Ti-magnetite grain. Moreover, the sulphide mineralization is likely of region-wide hydrothermal origin. The magnetizations carried by the pyrrhotite and magnetite have nearly identical directions and so, must be nearly of the same age. For this study, we sampled 56 sites including 39 dykes, 10 baked-contact rocks and 7 host rocks removed from the immediate dyke contacts. The dykes and the contact rocks have the same SW and up directions of magnetization, and contain the Fe-sulphide or the magnetite magnetization or both, as diagnosed by their relative unblocking temperatures. However, all the sampled carbonate and igneous host rocks far away from the dykes also have the same directions. Thus, all of the 10 originally planned contact tests are inconclusive. The new palaeopoles of this study are a few degrees apart; the magnetite pole (from dykes only, $N = 25$) is located at 51°N , 164°E , $K = 69$, $A_{95} = 3.5^\circ$, whereas the pole calculated from iron sulphide magnetic directions (all rock types, $N = 20$) is at 54°N , 166°E , $K = 112$, $A_{95} = 3.1^\circ$. All directions are of reversed polarity, suggesting that the magnetization was acquired during the Kiaman Reversed Superchron. The palaeomagnetic mean result from the magnetite-bearing sites implies a palaeolatitude of Oslo of 23°N , whereas the palaeolatitude calculated from the pyrrhotite magnetizations is $25\text{--}27^\circ\text{N}$, depending on choice of host lithologies.

As noted in many previous publications, the palaeomagnetic poles for the late Palaeozoic and Early-Middle Triassic are in conflict with classical Pangea reconstructions. The poles with ages of 250 ± 10 Ma, in particular, previously showed a discrepancy of some 25° or more, when the Gondwana and Laurussia continents are restored to their juxtapositions in the Pangea-A fit, before the opening of the Atlantic Ocean. Proposed solutions to this conundrum have been controversial, involving doubts about (1) the geocentric coaxial dipole field model,

(2) the reliability of the palaeomagnetic results or their ages, or (3) the validity of the Pangea-A reconstruction, leading to proposals of a Pangea B reconstruction in which Gondwana is displaced some 3500 km to the east with respect to Laurussia.

The significance of our new result for this Pangea controversy resides in its improved age within an early Guadalupian (mid to late Permian) time interval where few results exist from well-dated igneous rocks in either Baltica or Laurentia. There are quite a few results from sedimentary rocks, but these may be suspected to suffer inclination shallowing, and are therefore less suitable to settle a palaeolatitudinal argument. Our new result of the magnetite magnetization, granted it is primary and acquired at about 270 Ma, combined with a new ~265 Ma result from Argentina and selected other poles from igneous rocks, leaves enough room for the north–south configuration of Pangea A at 270 Ma and avoids the overlap between Baltica and Gondwana that necessitated Pangea B, at least for the Late Permian.

Key words: Palaeomagnetism applied to tectonics.

INTRODUCTION

Nearly a century ago, Alfred Wegener proposed a supercontinental configuration called Pangea, in which the Atlantic Ocean is closed between Norway and Greenland, between Portugal and Newfoundland, between the West African and Atlantic coast margin of North America and between South America and Africa. Improvements in the precision of the reconstruction were made by Bullard *et al.* (1965) using a computer-aided minimization of gaps and overlaps. Subsequently this fit has been called Pangea A, and it remains to this day the most commonly portrayed Pangea reconstruction in introductory geosciences textbooks. However, a persistent problem involves the palaeomagnetic data for Permian and Triassic times: it has long been known that the available palaeopoles, especially for the interval of 270–230 Ma are rather disparate, when restored to Pangea-A coordinates (e.g. Irving 1967, 1977, 2004; Zijdeveld *et al.* 1970; Van Der Voo & French 1974; Hallam 1983; Van Der Voo *et al.* 1984; Smith & Livermore 1991; Muttoni *et al.* 1996, 2003; Torcq *et al.* 1997; Rochette & Vandamme 2001; Torsvik & Cocks 2004; Meijers *et al.* 2010; Yuan *et al.* 2011). In Torsvik *et al.* (2008), this is portrayed (their fig. 6b) by means of apparent polar wander paths (APWPs) for Gondwana and Laurussia, which are seen as reaching their maximum separation of some 25° or more at about 250 ± 10 Ma, despite being reconstructed in Pangea A with the Atlantic Ocean tightly closed. Another way to portray the discrepancy is to keep the continents in the same longitudinal positions as occupied within Pangea A, but to let their latitudinal positions be determined by the palaeomagnetically determined palaeolatitudes; this produces an overlap in the north–south sense of some 11° (Fig. 1).

Attempts to reduce this misfit have been controversial, and were proposed because of doubts about (1) the geocentric coaxial dipole field model (Briden *et al.* 1971; Van Der Voo & Torsvik 2001), or (2) the reliability of the palaeomagnetic results or their ages (e.g. Rochette & Vandamme 2001), or (3) the validity of the Pangea-A reconstruction, leading to proposals of a Pangea B reconstruction in which Gondwana is displaced some 3500 km with respect to Laurussia (e.g. Irving 1977, 2004 and many references therein; Muttoni *et al.* 1996, 2003).

In general, reception of this last proposal has been lukewarm to negative by the geological community (e.g. Hallam 1983), not in the least because Pangea B must have transformed into a Pangea-A type reconstruction well before the Atlantic Ocean opened at ~180 Ma. This transformation requires an intra-Pangean dextral megashear along a 3500-km-long fault zone, running ENE–WSW between

Laurussia and Gondwana, with the Iberian Peninsula and Florida in somewhat uncomfortable transpressional positions straddling the fault zone.

The timing of the movement along this megashear is also controversial: Muttoni *et al.* (1996, 2003) have argued that it is best placed in middle Permian times, whereas Irving (1977) and Torcq *et al.* (1997) have placed the movement in the Triassic. Given that the logical locations of the megashear zone do not follow a perfect small circle, one would expect some major transpression and transtension to occur in and adjacent to the zone, but observations do not confirm this. In fact, Weil *et al.* (2001) have shown that displacements along a WSW–NNE oriented fault zone in Iberia would most likely be sinistral instead of dextral as needed for the intra-Pangean megashear.

Agreeing with Rochette & Vandamme (2001), Van Der Voo & Torsvik (2004) have emphasized that there are many potential sources of error that can affect the palaeomagnetic poles and corresponding palaeogeographic locations of a continent. In a detailed analysis of the Permian and Triassic palaeomagnetic data from stable Europe ('Baltica'), they concluded that the poles of the European craton are no exception. These errors can be divided into random ones or 'noise', and systematic errors or bias.

Random departures from a mean direction, such as secular variation, can be reduced by time averaging their effects. Systematic errors, on the other hand, can escape detection. If they are recognized, however, they can be controlled to a greater extent than the random errors since the systematic ones are primarily caused by one or more of a small number of causes, for which the magnitude can be estimated. These causes can include inclination shallowing in the magnetic record of sedimentary formations, errors in age assignments, erroneous tilt corrections and contaminations by more recent overprints superposed on primary magnetizations acquired during a long period of one polarity (such as the Kiaman Reversed Superchron). Van Der Voo & Torsvik (2004) showed that any of these four systematic errors would produce a more southerly palaeoposition for Europe than is warranted, and this could be the cause of a large overlap (Fig. 1) in a longitudinally constrained Pangea A configuration (Muttoni *et al.* 2003).

Our study attempts to reduce the above-mentioned biasing effects by using mainly well-dated volcanic rocks, with demonstrably reliable demagnetization behaviour. Thus, we argue that a modern comparison of palaeopoles to test Pangea reconstructions should exclude sedimentary and poorly dated results, as well as data not based on careful demagnetizations that include principal component analysis.

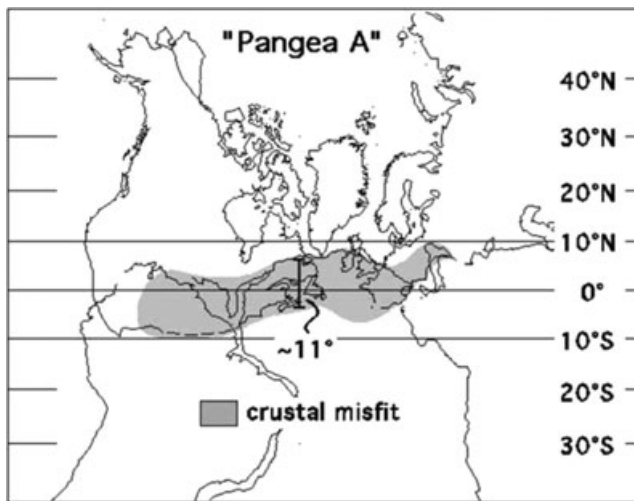


Figure 1. Overlap during the Early Permian (~280 Ma) in a configuration that keeps the Gondwana and Laurussia continents in the same longitudinal positions as Pangea A, but adjusts their palaeolatitudes according to the available palaeomagnetic data compiled by Muttoni *et al.* (2003). Reproduced with permission of Elsevier Publishing Co.

GEOLOGICAL SETTING

During the Silurian, when western Scandinavia was situated in central Laurussia, it was located in a tropical palaeolatitude, allowing for the formation of widespread shallow-marine limestone deposits teeming with brachiopods (Cocks & Worsley 1993). These limestones now form the country rock in much of this study's sampling region (Fig. 2).

At this time, the area around Oslo became a foreland subject to folding and thrusting related to the Caledonian orogeny, which deformed Cambro-Silurian sediments near our study area and in a larger context juxtaposed Laurentia, Baltica and Avalonia in a combined Laurussia continental element. Then at approximately 330 Ma, Gondwana and Laurussia began their protracted collision, culminating in the Pangea supercontinent. Well before Pangea began to break apart, southwestern Scandinavia underwent rifting in different locations (Brekke *et al.* 2001; Mosar *et al.* 2002). The Oslo Rift is situated in the northern section of the Rotliegendes (early-to-mid Permian) Basin in Europe (Larsen *et al.* 2008). According to several authors (Ramberg & Larsen 1978; Sundvoll *et al.* 1990; Sundvoll & Larsen 1993; Olausson *et al.* 1994), the Oslo Graben evolved in five phases. In the first phase, the Asker Group sediments, inferred to be deposits of a fluvial-deltaic environment, were unconformably deposited on a pre-Caledonian Cambro-Silurian sequence. The Group's age is constrained to be Serpukhovian–Moscovian (~317 ± 10 Ma), based on foraminifera and U-Pb dating of detrital zircons (Henningsmoen 1978; Olausson 1981; Olausson *et al.* 1994; Dahlgren & Corfu 2001). When rifting began, there was a significant intrusive activity consisting of trachy-andesitic-rhyolitic sills and dykes, having Rb-Sr ages of 304 ± 8 and 294 ± 7 Ma (Ramberg & Larsen 1978; Sundvoll *et al.* 1992). Rifting did not show its typical topographic development in the Oslo region until the Early Permian, when there was vertical displacement along faults, and trachy-andesitic rhomb-porphry lavas erupted from the vents produced by this displacement (Ramberg & Larsen 1978). Eventually, the graben began to collapse, while still containing central volcanoes, along with the formation of linear as well as ring dykes (Heeremans 2005). The final (fifth) stage of graben development involved the emplacement of intermediate to silicic intrusions

(e.g. larvikites and syenites). Parts of these intrusions were derived from partial melting of the crust.

Dyke formation, then, was widespread throughout the entire progression of the Oslo Graben magmatism. However, the latest dyke intrusions are of particular interest for palaeomagnetic tests of Pangea configurations, because of their ages spanning Late Permian to Early Triassic times; it is precisely for the 270–240 Ma interval that the palaeomagnetic database appears to be in greatest need of improvement, because there are not enough well-dated palaeopoles from volcanic rocks in stable regions for this time.

The later rifting between Greenland and Scandinavia caused breakup and the formation of the Northeast Atlantic Ocean in the Early Cenozoic at about 54 Ma (Torsvik & Cocks 2005). However, the Oslo area remained a stable part of the Baltic shield ever since Permian igneous activity ceased. This stability implies that no regional tilting occurred after intrusion of the dykes.

SAMPLING

We collected 472 samples with a gasoline-powered portable drill in 2005 August. This includes 56 sites total, including 39 intermediate to mafic dykes and 10 sites in what can be inferred as the baked contacts of these dykes, that is, well within the expected thermal aureole of the intrusions (within one dyke width). Most of these contacts were early Palaeozoic limestones, but a few consist of Early Permian igneous intrusive or extrusive rocks. The contact limestones were sampled in close proximity to the dykes, whereas unbaked (and presumably unaffected) host rocks were collected at an additional seven sites at a distance from the dykes where they could not have been thermally remagnetized by the intrusive event. A compass and inclinometer were used to determine the azimuth and the plunge of the core samples; solar compass readings were taken as well when the weather permitted it. The readings of azimuths with the solar compass showed that magnetic intensities were not high enough to affect orientation measurements with a compass. A correction for the magnetic deviation of 0° 51'E has been made to all relevant measurements.

Fig. 2 shows the distribution of the sampling sites ranging from downtown Oslo (sites 1–4) to Ingelstad in the vicinity of the town of Brandbu, some 40 km to the north-northwest. The greatest concentration of dykes, and hence, our sampling sites, is west of Roa in the vicinity of road 35 towards Jevnaker (Fig. 2).

LABORATORY METHODS

Standard 2.2-cm-high cylindrical specimens were cut from the field-drilled cores. Specimens that were broken were treated with an alumina cement which, even after heating, does not affect the magnetic readings in the magnetometer. The natural remanent magnetization (NRM) of the rocks was measured using a three-axis 2G superconducting magnetometer, housed inside a shielded room with rest-field less than 200 nT. Most specimens were thermally demagnetized up to 580 °C in an ASC TD-48 demagnetizer inside the shielded room, whereas alternating field (AF) demagnetization up to 200 mT was carried out on some pilot samples with a Sapphire Instruments SI-4 demagnetizer. Although AF demagnetization results resembled those obtained thermally, thermal demagnetization was typically more successful in isolating the characteristic magnetization, and was therefore the treatment of choice. Orthogonal vector endpoint diagrams (Zijderveld 1967), stereographic projections and principal component analysis (Kirschvink 1980) were used to determine the

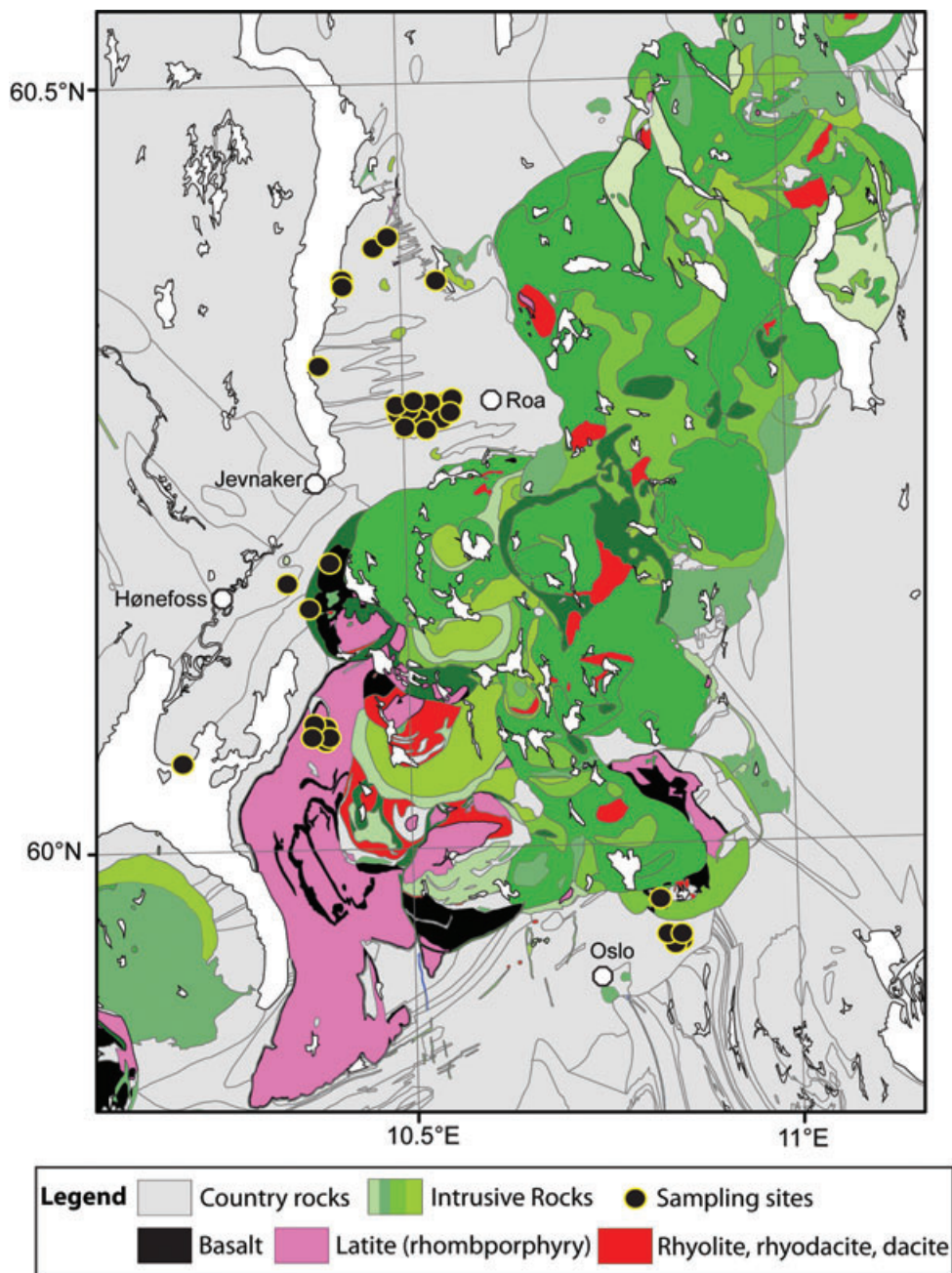


Figure 2. Map of the igneous complexes, country rocks and tectonic relationship of the northern part of the Oslo graben, with sampling sites indicated. See Tables S1 and S2 for GPS coordinates. Figure adapted from the Norwegian Geological Survey GIS database.

directions of the characteristic magnetizations. The analysis used the Super-IAPD (Torsvik *et al.* 2000) and Palaeomac (Cogné 2003) software. The principal component analysis calculations included the Maximum Angular Deviation (MAD) of the components that make up the remanence. Specimen directions, sample and site numbers, MADs and GPS coordinates are included in the Supporting Information (Tables S1 and S2). Results from some 34 specimens with $MAD > 15^\circ$ were rejected and excluded from sample-mean, site-mean and overall mean calculations.

Identification of the magnetic carriers was aided by low-temperature remanence and high-temperature susceptibility experiments conducted on a Magnetic Properties Measurement System (MPMS) and a susceptibility-bridge at the Institute for Rock Mag-

netism at the University of Minnesota. The MPMS measured the change in the saturation remanence, imparted at room temperature before cycling down to liquid-helium temperatures and back. The coercivity of the carriers was characterized by means of hysteresis loops run on a vibrating sample magnetometer at the University of Minnesota as well as acquisition experiments of isothermal remanent magnetizations (IRMs), performed with an ASC Scientific Model IM-10-30 Impulse Magnetizer at the University of Michigan for a small selection of specimens.

To image the most likely carriers of the magnetization, a scanning electron microscope [SEM, Hitachi, fitted with an energy-dispersive analysis system (EDS)] was used to qualitatively assess their occurrences. Afterwards, an electron microprobe (Cameca SX-100) was

used to refine the composition of potential magnetic carriers (Fe-oxide or pyrrhotites).

$^{40}\text{Ar}/^{39}\text{Ar}$ age dating and mineral separation used standard techniques in the $^{40}\text{Ar}/^{39}\text{Ar}$ Geochronology Laboratory of the Norwegian Geological Survey (NGU) in Trondheim. Before packing in Al-foil, mineral separates were handpicked under a binocular microscope and all samples were rinsed in alternating acetone and distilled water. The sample packets were stacked and loaded in a sealed Al-capsule with Cd-shielding for irradiation in the 5C site at the McMaster Nuclear Reactor facility, Hamilton, Canada. The samples were irradiated at McMaster for 16h40m at 3 MW (50 MWH) with nominal neutron flux of $4 \times 10^{13} \text{ n (cm}^2 \text{ s)}^{-1}$; nominal temperature in the irradiation site is $<50 \text{ }^\circ\text{C}$ (M. Butler, personal communication, 2001). Production of isotopes from Ca and K were determined by irradiation of CaF and K_2SO_4 salts; values of $^{36}\text{Ca}/^{37}\text{Ca} = 0.000169$, $^{39}\text{Ca}/^{37}\text{Ca} = 0.000736$ and $^{40}\text{K}/^{39}\text{K} = 0.032593$ were used. Neutron fluence was monitored with Tinto biotite of 410.3 Ma (Rex & Guise 1995). We incorporated a conservative 1 per cent error in J -value for all unknowns.

Gas from irradiated samples was released in a step-wise fashion from a resistance furnace. Furnace conditions are similar to those described in Eide *et al.* (2002). Gas released from a sample at a single temperature step was cleaned in the extraction line for 11 min using two pairs of SAES AP-10 getters, mounted in isolated sections of the line, each maintained with their own vacuum pumps. The purified gas was then analysed on a MAP 215-50 mass spectrometer. Data for blanks, monitors and unknowns were collected on a Johnson electron multiplier with gain setting at 1, while the magnet was automatically scanned over masses ranging from 35 to 41 in a cycled, 'peak-hop' mode. Masses from 37 to 40 were each measured in 10 cycles and 10 counts per mass per cycle; mass 36 was measured with 20 counts per cycle.

Dynamic blank measurements on mass 40 indicate a stable background (1.0×10^{-13} ccSTP, where STP is standard temperature and pressure). Background levels (blanks) for the furnace were measured at 100–200 $^\circ\text{C}$ temperature increments prior to each sample analysis. Furnace blanks were maintained at levels less than 1.1×10^{-11} ccSTP for mass 40 and $3\text{--}5 \times 10^{-14}$ ccSTP for mass 36 at temperatures of 500–1000 $^\circ\text{C}$; blanks increased to 3.0×10^{-11} ccSTP for mass 40 and 1.1×10^{-13} ccSTP for mass 36 at high temperatures (1200–1400 $^\circ\text{C}$). Background levels of masses 37 and 39 did not change significantly from dynamic blank levels at any temperature (1×10^{-13} ccSTP for mass 37; $<5.3 \times 10^{-14}$ ccSTP for mass 39). Background levels for mass 38 were $<3 \times 10^{-14}$ ccSTP at all temperatures. At experimental temperatures between 600 and 1000 $^\circ\text{C}$, furnace blanks for mass 40 typically were <1 per cent of the sample signal size.

Data from unknowns were corrected for blanks prior to being reduced with the IAAA (Interactive Ar-Ar Analysis) software package (Visual Basic programming for Windows PC) written by T.H. Torsvik and N.O. Arnaud and based in part on equations in Dalrymple *et al.* (1981) and McDougall & Harrison (1999). Data reduction in IAAA incorporates corrections for interfering isotopes, mass discrimination (measured with an air pipette), error in blanks and decay of ^{37}Ar .

MAGNETIC MINERALOGY

Demagnetization characteristics of a large majority of the samples revealed two clearly distinguishable magnetic components in terms of intensity decay as a function of temperature (Fig. 3). A sharp drop in intensity is revealed between 300 and 350 $^\circ\text{C}$, followed by a

shoulder and then a final drop in intensity to near-zero remanence at 575 $^\circ\text{C}$ or less (Figs 3c and f). The corresponding trajectories in the orthogonal demagnetization diagrams (e.g. Fig. 3c) showed very slight differences in direction, with the first removed component having a tendency to be slightly steeper upwards by only a few degrees than the higher temperature component.

An IRM was imparted to a limestone sample with the $\sim 350 \text{ }^\circ\text{C}$ maximum unblocking temperatures in a near-saturation field of 1.1 T, followed by two lower field applications of 0.3 T and 0.12 T at right angles to the highest-field IRM. This 3-D IRM (Lowrie 1994) is then thermally demagnetized and this yields the unblocking temperature spectra of the coercivities involved in the IRM acquisition. The resulting plot (e.g. Fig. 4) reveals that the coercivity of the component acquired in 1.1 T minus the component acquired in 0.3 T is dominant and that its coercivities are higher than theoretically possible for magnetite. The unblocking temperatures of the entire IRM in this sample are between 300 and 350 $^\circ\text{C}$. All in all, this strongly suggests that this IRM is carried by pyrrhotite. Further evidence for pyrrhotite is seen in Fig. 5 where MPMS results of a sample (#115 from dyke site 14) yielded a diagnostic sudden change in remanence at $\sim 35 \text{ K}$ (Fig. 5 bottom panel); this transition can be due either to pyrrhotite ($\sim 35 \text{ K}$; Dekkers *et al.* 1989; Rochette *et al.* 1990) or siderite ($\sim 40 \text{ K}$; Housen *et al.* 1996), with pyrrhotite being the likely choice given the abundance of sulphides and a lack of iron carbonates in these dykes. In addition, two samples (#115 from dyke site 14 and 85 from dyke site 11) revealed a Verwey transition at about 115 K in MPMS runs (Fig. 5).

The observations with the microprobe and SEM, including the use of EDS, revealed an abundance of Fe-sulphide grains. In some cases, these were euhedral grains large enough to reveal their composition as pyrite (Fig. 6a), and sometimes they consisted of pyrite framboids (Fig. 6d). However, in other cases the Fe-sulphide grains were too small to determine the Fe-S ratio with confidence and these grains probably could include finely distributed pyrrhotite. Lending confidence to this conclusion are the earlier mentioned rock magnetic features (Figs 4 and 5), as well as the maximum unblocking temperatures up to 350 $^\circ\text{C}$ (Figs 3 and 4).

The presence of magnetite was confirmed by SEM and microprobe in samples 52 and 89. Several grains contained titanium, and some of these showed abundant exsolution lamellae (Figs 6b and c), which accounts for the typical maximum unblocking temperatures near $\sim 580 \text{ }^\circ\text{C}$ (e.g. Figs 3a and d), indicative of Ti-free magnetite as remanence carrier. Exsolution into ilmenite and low-Ti magnetite is generally thought to be a high-temperature deuteric oxidation process, occurring upon cooling from intrusion temperatures. These observations therefore confirm that the original Ti-Fe oxide is of primary, igneous origin. Furthermore, some feldspar grains were observed to contain Fe-rich oxide inclusions, occasionally with minor Ti, which is also indicative of a primary nature of the potentially magnetic oxides.

As already mentioned, some samples appeared to contain only pyrrhotite as the remanence carrier (Figs 3b and e), and other samples had only magnetite as the carrier (Figs 3a and d), but quite commonly samples contained both. That the Fe-sulphides are secondary in the dykes (as well as the limestones, see Fig. 6d) is suggested by the side-by-side occurrence of an iron-sulphide and a Ti-Fe oxide (Fig. 6a); here the texture of the titanomagnetite is continuing on either side of the sulphide intruding into its side. The coexistence of iron-sulphide and iron-oxide was best observed in thermal demagnetization (up to about 600 $^\circ\text{C}$) of the samples, because AF demagnetization up to 200 mT did not show the two-component nature of the remanence very well.

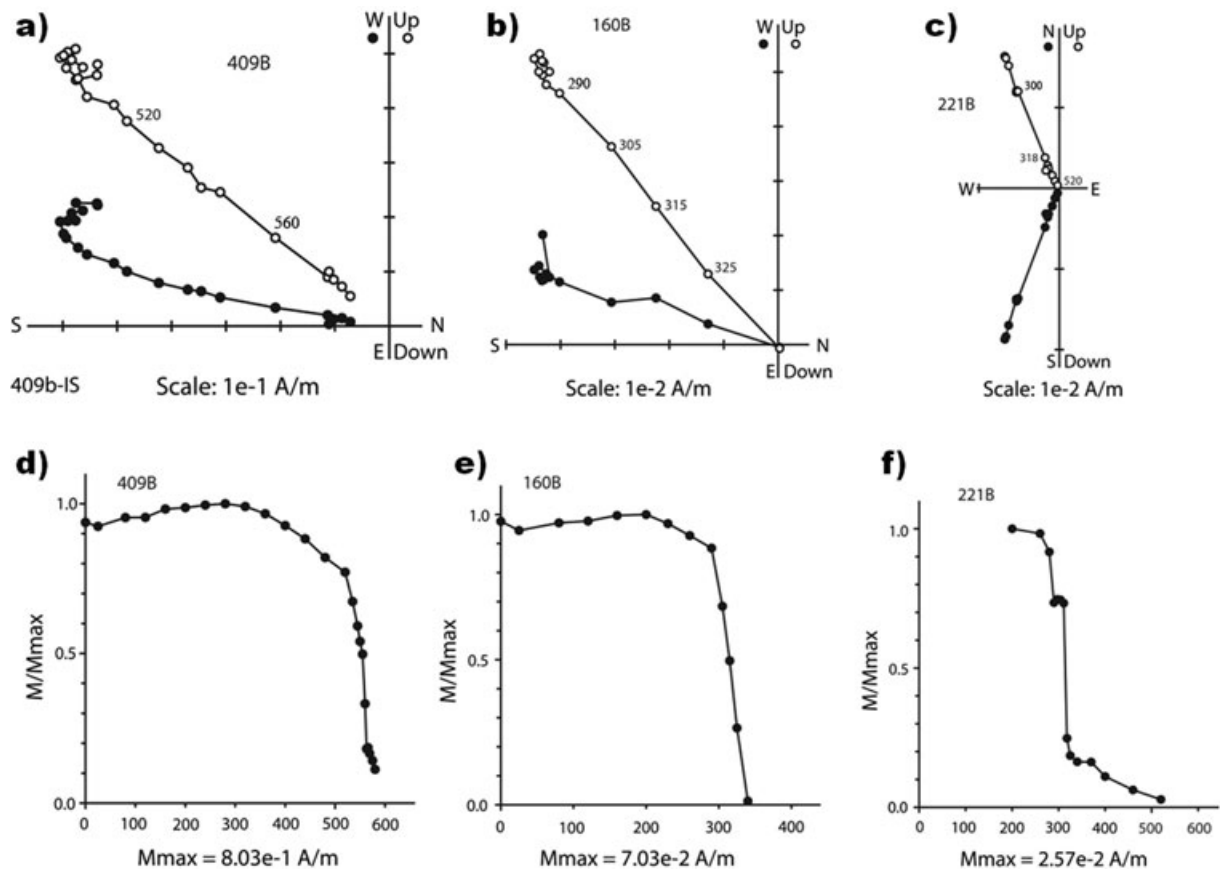


Figure 3. Magnetic components found in the samples from our study illustrated by Zijderveld diagrams representing (a) a sample containing magnetite, (b) a sample with iron sulphide component and (c) a sample with magnetite and iron sulphide present with nearly the same direction of magnetization. Remanence intensity versus temperature diagrams show (d) the unblocking temperatures up to 580 °C characteristic of magnetite in the sample in (a). Diagram (e) shows that the sample in (b) has a maximum unblocking temperature at approximately 340 °C, characteristic of Fe-sulphides. The diagram in (f) shows the unblocking in the sample shown in (c), where both magnetite and iron sulphide are recognizable by their characteristic unblocking temperatures.

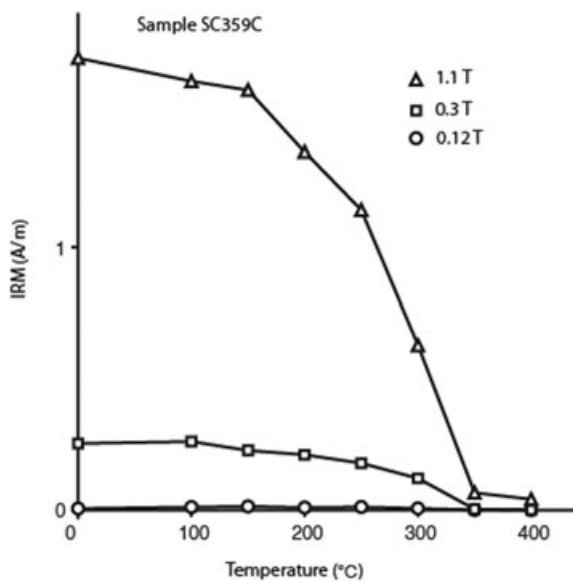


Figure 4. Thermal demagnetization of a 3-D IRM acquired in an orthogonal system with applications of fields of 1.1 T, 0.3 T and 0.12 T, sequentially (Lowrie 1994).

Bulk hysteresis properties of sample 85 (site 11), which is dominated by the lower coercivity component identified as low-Ti magnetite, suggest that the carriers predominantly lie in the pseudo-single domain (PSD) to multidomain (MD) grain size range ($M_{rs}/M_s = 0.08$ or higher and H_{cr}/H_c up to 5). However, such bulk properties can be misleading if a mixed assemblage of grain sizes are present, so an analysis of first-order reversal curves (FORCs) from this sample was also conducted. The FORC distribution (Fig. 7) is nearly symmetrical about the $H_u = 0$ axis, with a broad vertical spread along $H_c = 0$ and with contours that diverge towards the origin, which is diagnostic of MD grains (Roberts *et al.* 2000). However, there is a subtle, closed peak at $H_c = 13$ mT, $H_u = 0$, which may be an indication of a distinct population of single-domain (SD) sized grains, but more likely represents a fraction of the MD population that exhibits SD-like behaviour (i.e. PSD grains). In either case, a subset of the present grains have the capacity to carry a primary Permian remanence.

AGE DATING RESULTS

Early dating efforts of dykes in the sampled region with the Rb–Sr technique yielded ages of 249 ± 3 Ma (Sundvoll & Larsen 1993) and 268 ± 5 Ma (Sundvoll *et al.* 1990). Thus it has been suspected

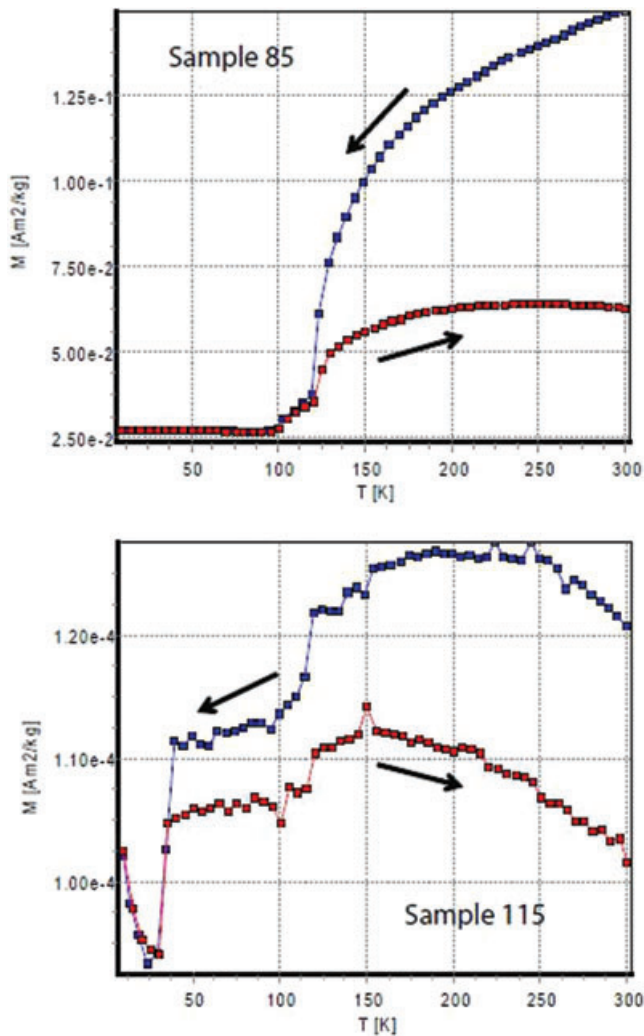


Figure 5. Remanent magnetization intensity upon cooling and heating (as indicated by the arrows) of sample 85 from a dyke at site 11, and sample 115 from a dyke at site 14, showing a sudden change in remanence at about 115 K, attributed to the Verwey transition in magnetite; moreover, sample 115 also shows a pronounced transition at 34 K, indicative of pyrrhotite. The saturation remanence is imparted at room temperature before cycling down to liquid-helium temperatures and back.

for some time with good reasons that such dykes intruded late in the history of the igneous activity of the Oslo Graben, in Late Permian to Early Triassic time. These and subsequent geochronological results for the dykes of interest to this study are summarized in Table 1.

More recent age dating (Torsvik *et al.* 1998) of these dyke rocks resulted in similar (Early Triassic) age dates. These authors included palaeomagnetic results for four Lunner dykes and performed ^{40}Ar - ^{39}Ar dating of two dykes, yielding ages of 237–246 Ma (their plateau age diagrams are shown in Fig. S1). Torsvik *et al.* (1998) noted that the ages for the individual steps in their spectra tended to increase at higher extraction temperatures. The 1σ uncertainties on the age of the individual steps were relatively large however (typically 2–3 per cent, compared to 1 per cent or less in our new results), so that under the conventional definition (>50 per cent of the cumulative ^{39}Ar in three consecutive steps that overlap at the 95 per cent confidence interval) their data could still be reported as true plateau ages. In effect, the relatively large (analytical) uncertainties in their analyses to a large degree masked an underlying trend of increasing ages.

Such a trend is generally considered indicative of (partial) argon loss, which would imply that the ‘plateau’ ages of 237–246 Ma are minimum ages only. Higher temperature steps in the three analyses by Torsvik *et al.* (1998) are older at 259.98 ± 12.04 Ma (2σ) for LU1A, 267.29 ± 11.02 Ma (2σ) for LU1 and 273.27 ± 11.86 Ma (2σ) to 289.79 ± 12.72 Ma (2σ) for sample LU4.

The two dykes studied by Torsvik *et al.* (1998) were resampled for our palaeomagnetic study as sites 16 and 20, with the latter yielding good palaeomagnetic directions. In a very recent study, Timmerman *et al.* (2009) obtained plateau ages of 246 ± 3 , 249 ± 3 and 273 ± 2.8 Ma, on a mafic and a syenitic dyke (see Table 1). The ages from this study are also all based on the $^{40}\text{Ar}/^{39}\text{Ar}$ method, with two of them (site 35 and 36) yielding statistically valid inverse isochron ages of 275.5 ± 5.4 Ma at 2σ (site 35; hornblende, Fig. 8) and 270.7 ± 2.6 Ma at 2σ (site 36; plagioclase, Fig. 9). In two samples collected at site 50 (whole rock, Fig. 10) the step ages vary too much to calculate a true spectrum or inverse isochron age, and therefore we resort to using the weighted mean ages of 267.5 ± 2.5 and 271.1 ± 2.5 Ma at 2σ (Table 1) for this site instead. We stress, though, that for the weighted mean ages there is more variation than can be explained by analytical uncertainty alone (Fig. 10). Details of the analyses are provided in Table S3.

We puzzled over the tendency of our new ^{40}Ar - ^{39}Ar age dates to be about 30 Myr older than those of the earlier efforts by Torsvik *et al.* (1998). Our new inverse isochron and weighted mean ages overlap with the higher temperature steps in the 1998 results, however, yielding support to the idea summarized earlier that the previously published ages (Torsvik *et al.* 1998) represent a case of (partial) resetting from an originally older age of ~270 Ma.

Three (younger) age dates pertain to sites 3 and 23 (Table 1, Sundvoll & Larsen 1993; Timmerman *et al.* 2009) from which we did, unfortunately, not retrieve any useful palaeomagnetic directions, so that their younger ages of 246–249 Ma do not allow us to couple it with any palaeomagnetic characteristics.

CRITERIA FOR REJECTION OF SPECIMEN DIRECTIONS

Tables S1 and S2 contain all component directions that could be identified by visual inspection of demagnetization diagrams followed by principal component analysis (Kirschvink 1980). Components listed in Table S1 were calculated over the unblocking temperature interval from 350 to 580 °C, and could generally be attributed to magnetite as their carrier. Components listed in Table S2 were calculated over the unblocking temperature range from 200 to 350 °C, and were attributed to pyrrhotite as their carrier. This mineral has the right characteristics to match our observations, as already discussed. Thus, if a specimen had a significant and sharp decay of the remanence just below 350 °C, we included its corresponding direction of magnetization in Table S2.

AF demagnetization up to 200 mT generally succeeded in eliminating a good part of the remanence (Fig. 11), regardless of lithology (dykes or limestones), but we suspect that it was more effective in demagnetizing magnetite than pyrrhotite. Whenever sister specimens of the same sample were demagnetized with AF and thermal treatments, the directions of the principal component analysis of the AF-demagnetized samples were typically slightly shallower than those demagnetized thermally. We conclude from this that a small fraction of a viscous overprint contaminates the higher steps in AF treatments, and we therefore prefer to use the results of thermally demagnetized specimens.

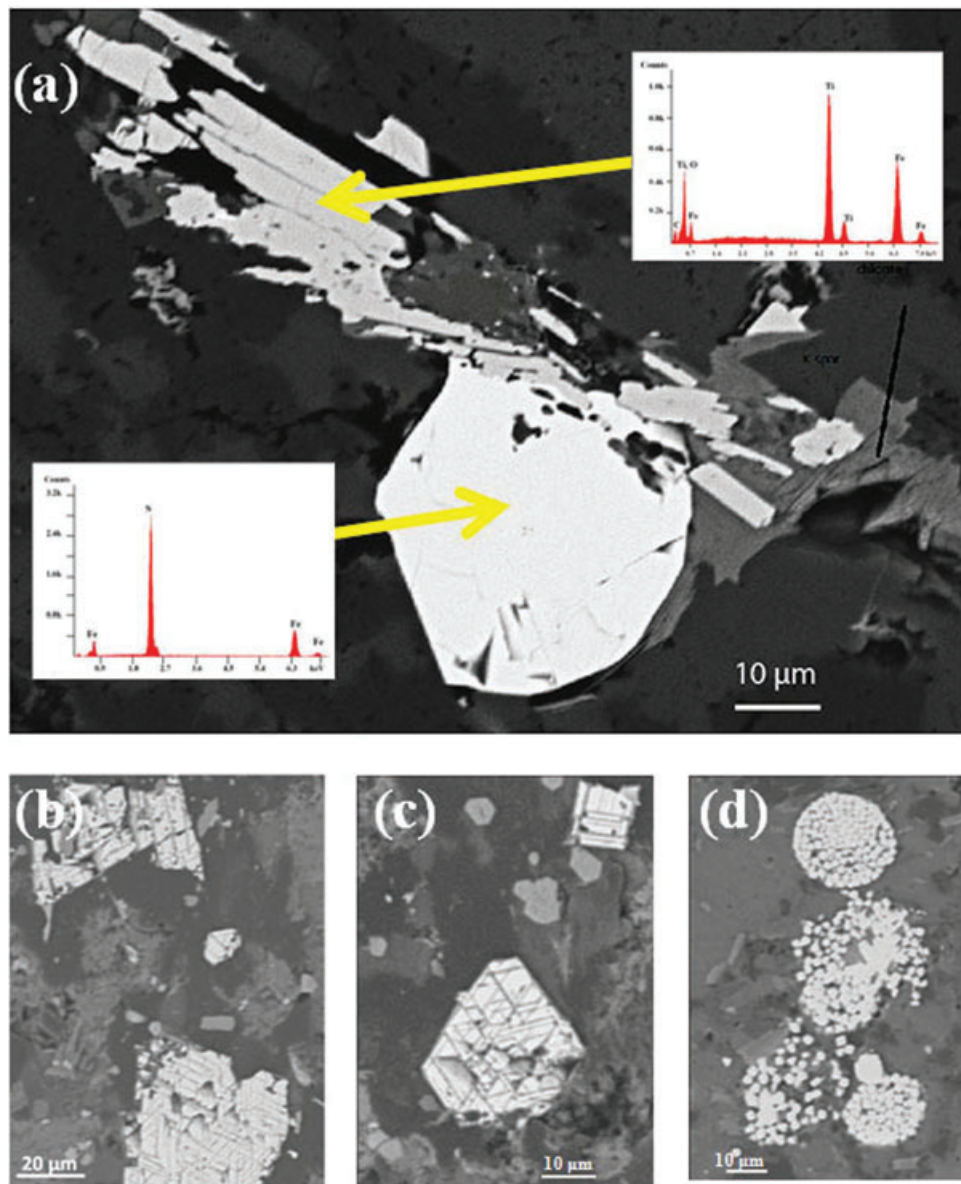


Figure 6. SEM images of iron-sulphides and titanium-iron-oxides. (a) Sample 52 (dyke, site 7) shows an Fe-sulphide grain (likely pyrite, lower EDS spectrum) invading a titanium-iron-oxide (upper EDS spectrum); the latter is inferred to be a primary igneous mineral, judging by its textural continuation on either side of the sulphide. (b and c) Examples of exsolution lamellae in sample 89 (dyke, site 11), interpreted as having formed upon cooling from intrusion temperatures. (d) Abundant pyrite framboids and crystallites in limestone sample (107, site 13).

When two specimens of the same sample gave component directions, they are both listed in bold face in Tables S1 and S2, with the note that these need to be combined before entering them in the list of sample directions, from which the site means of Table 2 are calculated in the next hierarchical level.

The directions of all the specimens in Tables S1 and S2 also include entries for specimens that gave anomalous directions (listed in red and in italics), which can also be inspected in Fig. S2(d). In this plot, it can be seen that these 74 anomalous directions define a random distribution spread over all quadrants other than the SW/up one (where the accepted directions reside). After subtracting the anomalous specimen directions, 522 entries remain, and of these 34 were associated with MAD angles greater than 15°; this latter threshold has been used as the angle above which directions are seen as unreliable and to be discarded. Figs S2(e) and (f) show examples of demagnetization diagrams of two specimens (10b from site 2 and

361b from site 42), where the MAD angle is just above 15° (see Table S2) resulting in rejection of their directions. One of these is for the magnetite component in specimen 10b, and the other for the pyrrhotite component in 361b.

Haematite, as diagnosed by unblocking temperatures in the range 580–680 °C, was observed in only two samples (367 and 368), both from site 43. The direction of the remanence carried by haematite in these samples conforms to that of the present-day field, from which we conclude that this haematite is a product of recent oxidation and does not influence the conclusions of this study.

One additional set of specimens excluded from the calculations of site-means deserves mention. These are labelled as contaminated by ‘too large an overprint’ in Tables S1 and S2. Such directions of magnetization, inferred to be influenced by large, but incompletely identified overprints, are usually streaked towards a downward or shallower upward direction because of overprinting

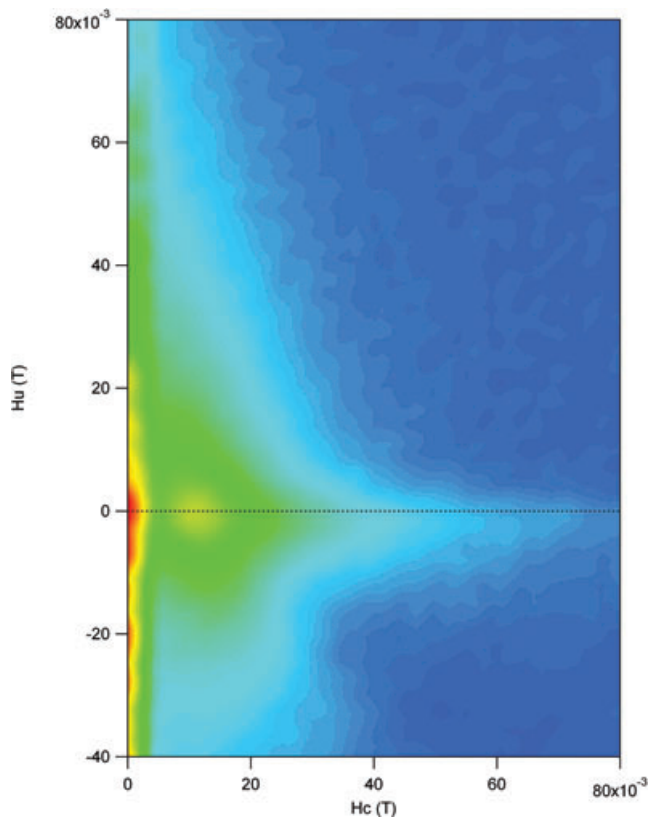


Figure 7. A first-order reversal curve (FORC) of sample 85 from a dyke at site 11, indicating multidomain and, more subtly (at $H_c = 13$ mT, $H_u = 0$), single-to pseudosingle domain grains.

by viscous records of the (steeply downward) present geomagnetic field. To remain conservative in the application of this rejection criterion, the number of samples so rejected totals only six (58a, 133a, 176a, 395b, 400a and 295a). Their inclusion, however, would have had a definite biasing effects on the site means; an example of the effect is given in Fig. S2(a)–(c), which illustrates this potentially important effect in a collection where all the directions are of the same polarity. It is worth noting that great-circle analysis is not useful in this regard because nearly all the directional trajectories parallel each other, and do therefore have no precision in their intersections.

Table 1. Age dates of the dykes of this study.

Site	Lithology	Location name, GPS	Method	Age (Ma)	Reference
3	Mafic dyke (VO2) (VO-3, kaersutite)	Vollebekk , Oslo City	Ar-Ar, Pl., phenocrist	246.0 ± 3.0	Timmerman <i>et al.</i> (2009)
		59.9385 10.8386	Ar-Ar, Pl., phenocrist	249.0 ± 2.4	Timmerman <i>et al.</i> (2009)
16	Intermediate dyke (Lu4)	W. Kalvsjotjernet 60.2896 10.5536	Ar-Ar, WMPA, WR	238.3 ± 4.5	Torsvik <i>et al.</i> (1998)
20	Intermediate dyke (Lu1 and Lu1a)	W. Kalvsjotjernet	Ar-Ar,WMPA	237.2 ± 4.4	Torsvik <i>et al.</i> (1998)
		60.2894 10.5525	WR, KFsp	246.2 ± 4.6	Torsvik <i>et al.</i> (1998)
23	Groerdite dyke (Storhaug dyke)	Linderudkollen 59.9646 10.8188	Rb-Sr	249.0 ± 3.0	Sundvoll & Larsen (1993)
34	Syenitic dyke (OC-3) Kaersutite phenocr.	Glisetra	Ar-Ar, Pl., phenocrist	273.0 ± 2.8	Timmerman <i>et al.</i> (2009)
		60.1877 10.3981			
35	Amfibole-rich dyke	Gjermundbo	Ar-Ar, hornblende, isochron	275.5 ± 2.7	This study
		60.1739 10.3426			
36	Ring dyke (Ringkollen syenite)	Øyangen	Ar-Ar, plagioclase, isochron	270.7 ± 2.6	This study
		60.1584 10.3705	Rb-Sr	268.0 ± 5.0	Sundvoll <i>et al.</i> (1990)
50	intermediate dyke	Bonsnes	Ar-Ar, WMA, leached WR	267.5 ± 2.5	This study
		60.0576 10.2035	Ar-Ar, WMA, unleached WR	271.1 ± 2.5	This study

Note: Pl., Plateau age; WMPA, Weighted mean plateau age; WMA, Weighted mean age; WR, whole rock.

In general, the directions from specimens with pyrrhotite components were somewhat less precise (average MAD = 6.6°), suffering more from lower temperature overprints than those of magnetite (average MAD = 4.0°). As mentioned, the components attributed to pyrrhotite as a carrier were calculated on the basis of their unblocking temperature range (up to 350°C), but spurious overprints or composite remanences eliminated in that same range may also have been included in Table S2. Component directions that deviated (by being located in a different quadrant) from the typical pyrrhotite (or magnetite) directions (southwesterly and up) have been labelled as ‘anomalous’ and were entered in italics in Tables S1 and S2. These were not included in the site-mean calculations, and were much more prevalent for the ‘pyrrhotite’ component than for the component attributable to magnetite. As a result, about twice as many pyrrhotite specimen components were rejected as being anomalous, or suffering from the overlapping effects of overprints, or because their MAD angle was greater than 15° . These rejections totalled 74 out of 250 specimens (rejection rate 29.6 per cent) for the pyrrhotite magnetization and 40 out of 346 specimens (rejection rate 11.6 per cent) for the magnetite components.

PALAEOMAGNETIC RESULTS

Fig. 3 shows representative Zijderveld diagrams of sample demagnetizations characteristic of magnetite, pyrrhotite or both, whereas Figs 12–14 illustrate the behaviour in thermal demagnetization of dyke samples and a sample of limestone not in proximity of an intrusion. As already mentioned, the plots of the normalized intensity of magnetization remaining after each step of treatment illustrate the unblocking temperature ranges that were used to attribute the remanence to either a pyrrhotite carrier or a low-Ti magnetite carrier, or both.

Table 2 lists the site-mean directions and statistical parameters, based on the data for the specimens in Tables S1 and S2. Mean directions for sites where magnetite is the carrier include only site-means based on three or more samples, whereas for the pyrrhotite carriers all sites with their corresponding specimen directions are included in Table 2, but those for $n = 1$ or $n = 2$ samples are given in italics. Table 3, in turn, lists the overall mean palaeopoles, with the corresponding statistical parameters. A variety of selection criteria and filters have been applied in the listed mean poles, but it can be seen that the variations are small and do not amount to more

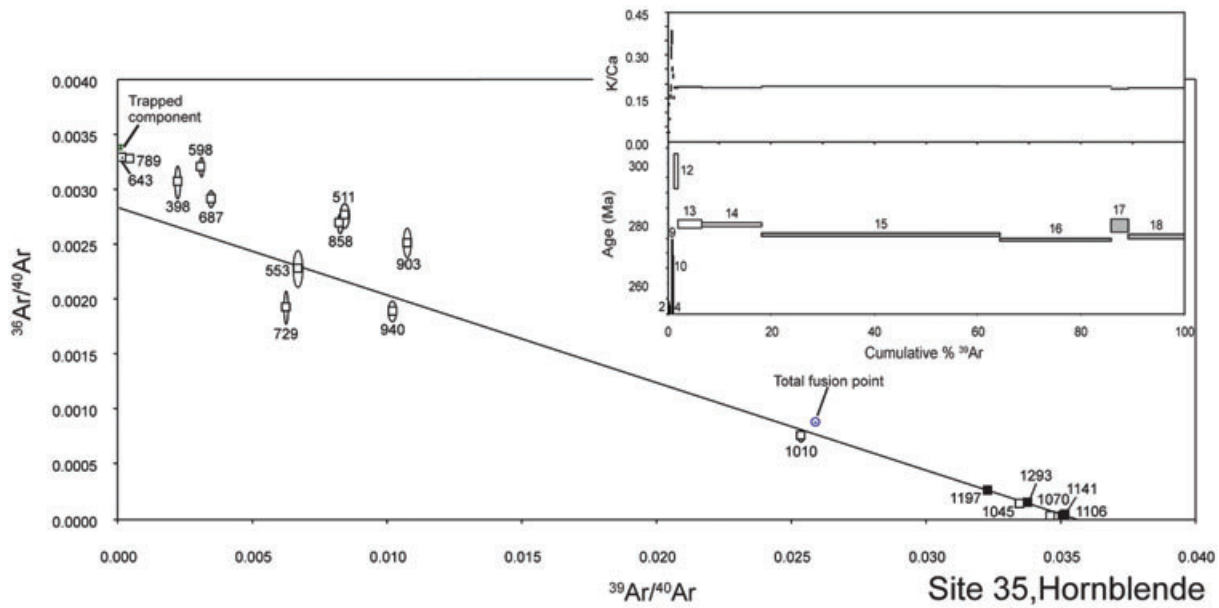


Figure 8. Age analysis of a hornblende separate from our sampling site 35, showing the inverse isochron and release spectrum. For steps 15–18 (1106 – 1293 °C; 81.9 per cent of the cumulative ^{39}Ar) an age of 275.5 ± 2.7 Ma (1σ) is obtained from the inverse isochron (MSWD 2.01; $^{40}\text{Ar}/^{36}\text{Ar}$ intercept of 328.0 ± 41.8 , i.e. overlapping the atmospheric ratio).

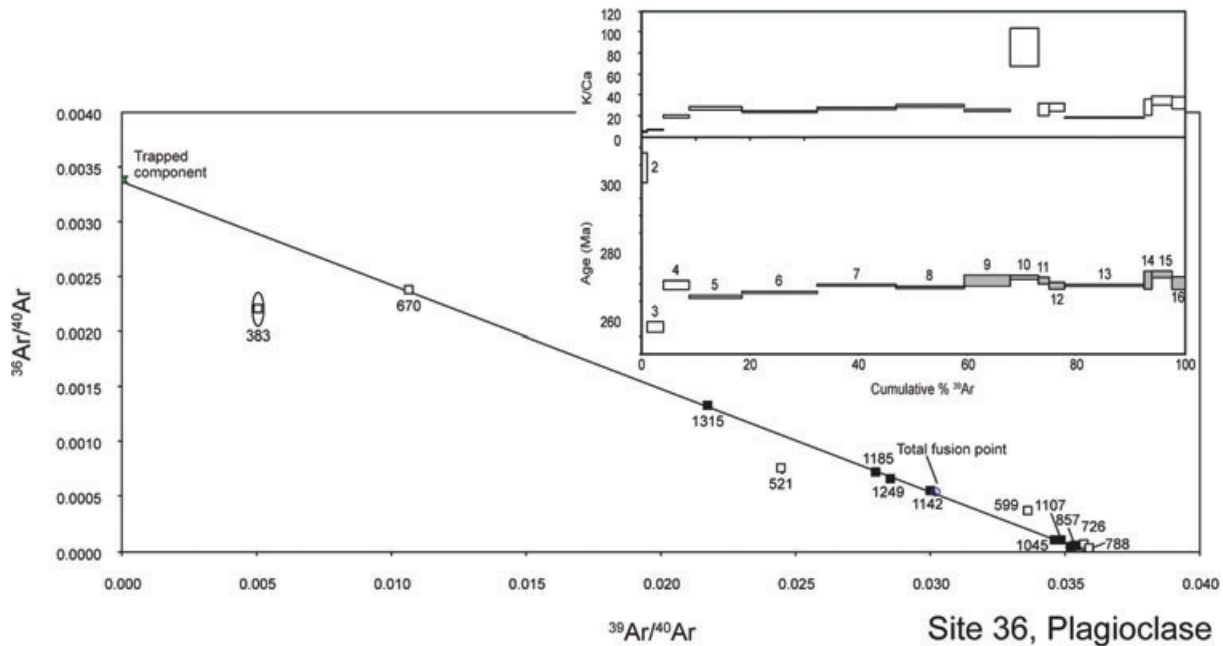


Figure 9. Age analysis of a plagioclase separate from our sampling site 36, showing the inverse isochron and release spectrum. The inverse isochron gives an age of 270.7 ± 2.6 Ma (1σ) for 67.7 per cent of the cumulative ^{39}Ar ; 857–1315 °C; MSWD 2.31; $^{40}\text{Ar}/^{36}\text{Ar}$ intercept 296.8 ± 3.7 , that is, overlapping atmospheric value at 95 per cent confidence interval. An earlier Rb-Sr dating yielded an age of 268 ± 5 Ma (Sundvoll *et al.* 1990). Magnetite carries the magnetization in this site.

than a couple degrees of (palaeo-) latitude. Site-means have been grouped according to remanence carrier, rock type and inclusion or exclusion of debatable results (e.g. where α_{95} , as associated with a given site mean, exceeds 15° , or where fewer than three samples are represented for a given site where pyrrhotite is the carrier). Site-means where magnetite is the remanence carrier have α_{95} 's uniformly less than 15° . Whenever the number of acceptable sample directions in a site with magnetite remanence is two or less,

no mean was calculated, as such a site should not carry the same weight in the overall calculation of the formation mean, as do more fully determined sites where at least three samples gave acceptable results.

All the accepted sites in Table 2 have a south-southwesterly and up direction (Figs 15 and 16), which in Baltica in the Permian or Triassic is a direction of unambiguously reversed polarity. No normal-polarity directions have been detected in any of the 482

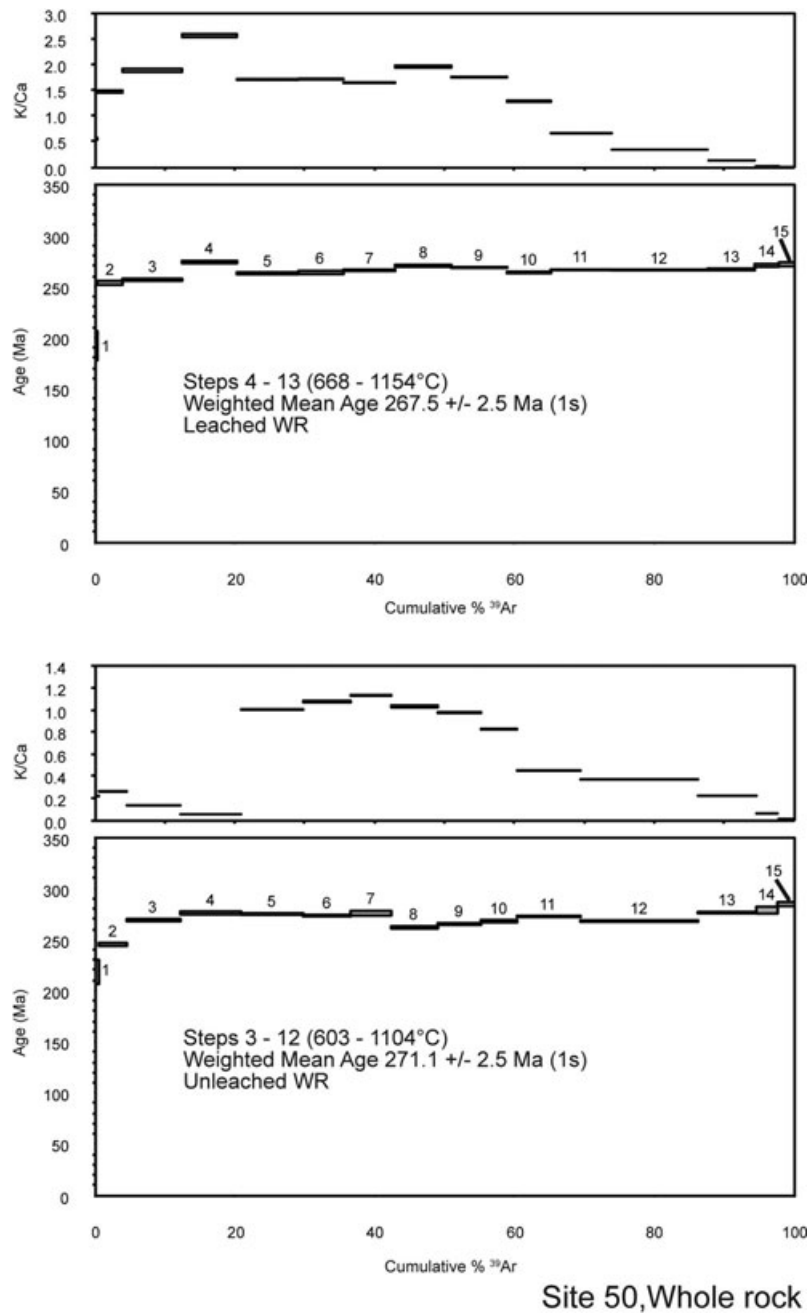


Figure 10. Age spectra for two whole rock analyses, site 50. Both spectra display more age variation than can be explained by analytical uncertainty alone. For the most stable part of these spectra we calculated weighted mean ages of 267.5 ± 2.5 and 271.1 ± 2.5 Ma, respectively.

accepted specimen directions. We will return to the significance of this polarity bias, when discussing the ages of the magnetite and pyrrhotite magnetizations.

Pyrrhotite and magnetite-hosted site-mean poles (Table 2) were used to calculate overall palaeopoles and their statistical parameters in various combinations (Table 3). Palaeopoles based on (1) dykes, (2) limestones in contact with dykes and (3) limestones far removed from the dykes can be seen separately in Table 3. It can be seen in the table that these palaeopoles are all very close together. When palaeolatitudes for a fixed point (Oslo at 60°N , 10°E) are calculated, they can be seen to range no more than $22.9\text{--}26.6^\circ$. With one exception, the cones of confidence (A_{95}) range from 2.5° to 5.6° , but

the differences are generally not statistically significant. The one exception, where $A_{95} = 8.8^\circ$, belongs to the mean palaeopole based on sites where pyrrhotite is the only carrier. The small number of sites ($N = 6$), when site-means based on fewer than two directions or having α_{95} values larger than 15° are excluded, is to blame for this larger A_{95} value.

CONTACT TESTS

Our purpose in collecting sites from dykes, baked contacts and host rocks was to complete a series of some seven or more baked-contact tests. For such a test to be positive, implying that the magnetization

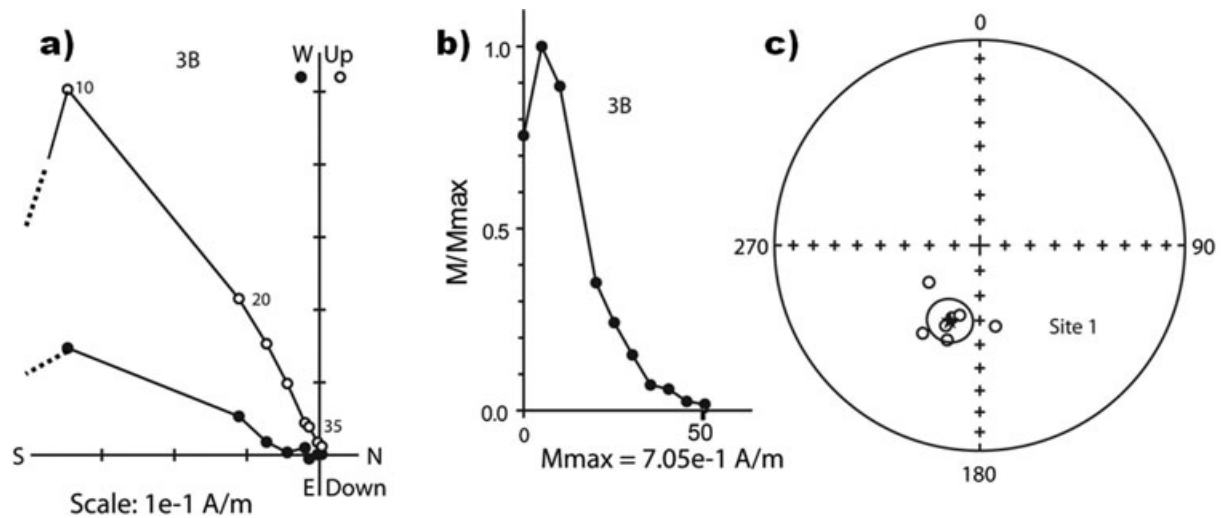


Figure 11. Alternating field (AF) demagnetization of a dyke sample (#3B) from site 1. (a) Zijderveld diagram depicting the directional trend, (b) intensity decay of sample 3B with increasing demagnetization steps (in mT) and (c) stereographic projection of the characteristic directions of all samples from this site (Site 1).

Table 2. Site-mean directions and virtual geomagnetic pole (VGP) positions.

Site	Type	Dec	Inc	<i>k</i>	α_{95}	<i>n</i>	G-Lat	G-Lon	V-Lat	V-Lon	dp	dm
Magnetizations carried by magnetite												
1	d	204.1	-59.7	42.8	8.6	8	59.9385	10.8386	65.5	142.4	9.8	13.0
5	d	204.8	-33.1	299.3	4.4	5	60.2830	10.5318	44.2	156.7	2.8	5.0
7	d	203.6	-37.7	43.9	8.4	8	60.2830	10.5318	47.5	157.0	5.8	9.9
9	lh	203.8	-36.7	13.0	12.0	13	60.2879	10.5466	46.7	147.1	8.2	14.0
10	d	201.5	-42.1	297.0	3.2	8	60.2879	10.5466	51.1	158.4	2.4	3.9
11	d	201.1	-38.5	91.9	5.8	8	60.2879	10.5466	48.6	160.1	4.5	7.2
12	d	199.2	-35.2	49.8	8.6	7	60.2880	10.5478	46.9	163.5	5.7	9.9
13	lc	203.6	-41.9	149.2	6.3	5	60.2880	10.5478	50.3	155.6	4.7	7.7
15	lh	199.5	-43.8	114.7	7.2	5	60.2880	10.5478	52.8	160.7	5.6	9.0
18	d	201.2	-42.9	83.9	6.1	8	60.2894	10.5525	51.7	158.6	4.8	7.7
20	d	196.5	-43.0	89.9	5.5	9	60.2894	10.5525	52.9	165.3	4.2	6.8
21	d	193.9	-29.4	76.1	14.2	3	60.2894	10.5525	44.3	171.7	8.7	15.7
22	d	198.2	-38.8	65.3	8.4	6	60.2894	10.5525	49.5	164.0	6.0	10.0
26	lc	205.3	-36.6	114.6	8.6	4	60.2880	10.5479	46.3	155.1	5.9	10.0
27	lh	202.8	-42.3	2470.0	1.5	5	60.2880	10.5479	50.9	156.6	1.1	1.8
28	d	203.0	-45.3	80.2	10.3	4	60.3160	10.3897	53.0	155.0	8.3	13.1
29	lc	204.2	-43.7	1023.0	2.4	5	60.3160	10.3897	51.5	154.0	1.9	3.0
30	d	203.6	-46.4	64.8	6.0	10	60.3920	10.4663	53.6	153.8	4.9	7.7
31	d	189.6	-37.6	268.8	4.1	6	60.3987	10.4831	50.1	176.4	2.8	4.8
32	d	228.1	-49.3	134.0	5.8	6	60.3697	10.5458	46.2	122.1	5.1	7.7
33	d	202.0	-42.2	149.5	3.7	11	60.3689	10.4235	50.9	157.6	2.8	4.5
34	d	177.9	-27.8	92.6	4.8	11	60.1877	10.3981	44.6	193.2	2.9	5.2
35	d	191.5	-29.3	35.5	8.8	9	60.1739	10.3426	44.7	174.7	5.4	9.7
36	d	195.2	-47.6	97.9	5.2	9	60.1584	10.3705	56.9	165.5	4.4	6.8
42	lh	199.3	-43.8	106.3	7.5	5	60.2849	10.5411	52.9	160.9	5.8	9.0
43	d	190.3	-39.7	599.4	3.1	5	60.0753	10.3940	51.8	174.9	2.2	3.7
44	d	197.6	-38.2	185.2	9.1	3	60.0753	10.3940	49.4	164.7	6.4	10.8
45	ic	192.7	-36.7	235.7	5.0	5	60.0753	10.3940	49.3	172.0	3.4	5.8
46	ih	195.2	-40.5	420.1	2.9	7	60.0753	10.3940	51.5	167.6	2.1	3.5
47	d	190.2	-42.5	261.1	4.2	6	60.0753	10.3944	53.8	174.6	3.2	5.2
48	d	192.7	-32.0	643.2	3.0	5	60.0753	10.3942	46.3	172.7	1.9	3.4
49	ic	192.0	-38.5	1031.0	1.7	8	60.0753	10.3942	50.7	172.6	1.2	2.0
50	d	190.8	-38.3	83.0	5.3	10	60.0576	10.2035	50.7	174.2	3.7	6.3
51	lh	189.4	-45.1	220.0	3.7	8	60.0576	10.2035	56.0	175.1	3.0	4.7
52	d	198.6	-48.0	121.3	4.4	10	60.3694	10.4242	56.3	160.3	3.8	5.7
53	d	199.1	-30.6	72.1	6.1	9	60.2940	10.5687	44.1	164.7	3.8	6.8
54	lc	203.6	-43.4	200.2	4.7	6	60.2940	10.5687	51.4	155.1	3.6	5.8
55	lh	198.6	-43.1	136.2	4.8	8	60.2940	10.5687	52.5	162.2	3.7	6.0

Table 2. (continued)

Site	Type	Dec	Inc	k	α_{95}	n	G-Lat	G-Lon	V-Lat	V-Lon	dp	dm
Magnetizations carried by Fe-sulphide												
2*	ic	<i>200.8</i>	<i>-54.4</i>			1	59.9385	10.8386	<i>61.6</i>	<i>153.1</i>		
4*	lc	<i>189.3</i>	<i>-51.8</i>			2	59.9385	10.8386	<i>61.8</i>	<i>174.1</i>		
5*	d	<i>208.8</i>	<i>-40.0</i>			1	60.2830	10.5318	<i>47.4</i>	<i>149.5</i>		
6	d	195.4	-42.2	35.5	11.4	6	60.2830	10.5318	52.6	167.1	8.6	14.0
7	d	199.6	-41.9	102.0	4.8	10	60.2830	10.5318	51.4	161.1	3.6	5.9
8*	d	<i>218.0</i>	<i>-36.0</i>			1	60.2832	10.5329	<i>41.6</i>	<i>139.9</i>		
9	lh	200.6	-41.5	61.0	5.1	14	60.2879	10.5466	50.9	159.9	3.8	6.2
10	d	198.8	-46.7	206.8	3.9	8	60.2879	10.5466	55.2	160.6	3.2	5.0
13	lc	195.7	-48.3	219.9	5.2	5	60.2880	10.5478	57.3	164.7	4.5	6.8
14	d	191.3	-43.5	21.8	13.2	7	60.2880	10.5478	54.2	172.9	10.2	16.4
15	lh	189.3	-49.1	74.7	8.9	5	60.2880	10.5478	59.1	174.7	7.8	11.8
18	d	202.4	-43.7	107.9	5.8	7	60.2894	10.5525	52.0	156.6	4.5	7.2
19	d	210.0	-36.8	33.9	13.3	5	60.2894	10.5525	44.9	149.1	9.1	15.6
21*	d	<i>200.9</i>	<i>-40.2</i>	<i>33.5</i>	<i>21.6</i>	3	60.2894	10.5525	<i>49.9</i>	<i>159.9</i>	<i>15.7</i>	<i>26.0</i>
22	d	182.8	-46.1	52.4	10.7	5	60.2894	10.5525	57.1	186.0	8.8	13.7
23*	d	<i>215.0</i>	<i>-28.0</i>			2	59.9646	10.8188	<i>38.2</i>	<i>145.9</i>		
24	d	191.6	-42.6	143.4	4.0	10	60.2875	10.5490	53.5	172.7	3.0	4.9
25	d	194.5	-35.2	118.4	4.5	10	60.2880	10.5479	47.9	169.9	3.0	5.2
26	lc	201.2	-40.5	448.6	3.2	6	60.2880	10.5479	50.0	159.4	2.3	3.9
27	lh	198.6	-44.5	375.4	3.5	6	60.2880	10.5479	53.6	161.7	2.8	4.4
29*	d	<i>176.9</i>	<i>-38.5</i>			1	60.3160	10.3897	<i>51.3</i>	<i>195.0</i>		
31	d	185.0	-38.8	391.0	4.7	4	60.3987	10.4831	51.3	183.0	3.3	5.6
32*	d	<i>213.0</i>	<i>-56.0</i>			1	60.3697	10.5458	<i>58.3</i>	<i>134.2</i>		
35*	d	<i>199.5</i>	<i>-33.5</i>			2	60.1739	10.3426	<i>45.9</i>	<i>163.3</i>		
37*	d	<i>202.9</i>	<i>-44.4</i>	<i>20.5</i>	<i>27.9</i>	3	60.2842	10.5390	<i>52.4</i>	<i>155.6</i>	<i>22.0</i>	<i>35.1</i>
38	lc	<i>204.9</i>	<i>-47.1</i>	<i>37.3</i>	<i>15.3</i>	4	60.2842	10.5390	<i>53.8</i>	<i>151.6</i>	<i>12.8</i>	<i>19.8</i>
39*	d	<i>196.7</i>	<i>-36.5</i>			1	60.2848	10.5409	<i>48.3</i>	<i>166.6</i>		
40*	lc	<i>190.5</i>	<i>-39.0</i>			2	60.2848	10.5410	<i>51.1</i>	<i>175.0</i>		
41*	d	<i>185.8</i>	<i>-26.6</i>			2	60.2849	10.5410	<i>43.6</i>	<i>182.8</i>		
42	lh	191.0	-47.6	79.5	6.8	7	60.2849	10.5411	57.5	172.4	5.8	8.8
51	lh	188.6	-40.1	131.9	4.8	8	60.0576	10.2035	52.3	177.2	3.5	5.8
53*	d	<i>205.2</i>	<i>-41.1</i>	<i>37.4</i>	<i>20.5</i>	3	60.2940	10.5687	<i>49.3</i>	<i>153.8</i>	<i>15.2</i>	<i>24.9</i>
54	lc	198.2	-44.2	1191.0	1.9	6	60.2940	10.5687	53.4	162.4	1.5	2.4
55	lh	194.3	-46.3	260.7	3.4	8	60.2940	10.5687	55.9	167.6	2.8	4.4
56	d	210.3	-58.4	57.3	10.2	5	60.2814	10.5281	61.6	135.0	11.2	15.1

Notes:

Mean directions based on $n = 2$ or less have not been included for magnetizations carried by magnetite.

Rock types: d, dyke; ic, igneous in contact with dyke; lh, igneous host rock away from dykes.

Lc, limestone in contact with dyke; lh, limestone host away from dykes.

G = GPS, global positioning system coordinates; V = VGP, Virtual geomagnetic pole; Lat, latitude; Lon, longitude; dp & dm, semi-minor and semi-major axes of oval of 95 per cent confidence.

*Mean directions with $\alpha_{95} > 15^\circ$, or with $n = 2$ or less are listed in italics. In the mean palaeopoles of Table 3, these have been excluded for the most selective entries.

dates to the time of intrusion, the characteristic remanence (ChRM) direction of a dyke is expected to be seen also in its baked contact, progressively diminishing in its contribution to the total remanence as the distance from the dyke margin increases. For a contact test to be fully convincing, host rocks should have a different ChRM direction outside the zone of thermal influence, proving that the dyke-plus-contact magnetization is younger and that region-wide remagnetization has not occurred. It is clear, though, from the preceding discussion and the palaeopole positions in Table 3 that the last stipulation is not satisfactorily met for our results and that the contact tests are, at best, inconclusive. Although it is indeed observed that contact rocks carry, within error limits, the same remanence as the dykes, the host rocks far removed are also carrying the same direction (see Fig. 15). Regardless whether these host or contact rocks are Silurian limestone, Permian syenite or Early Permian rhombporphyry, all the rocks have the same direction of magnetization as

the dykes, which suggests that some or all of these rocks have become remagnetized after their formation. As it turns out, many host limestone (lh) and contact limestone (lc) rocks have pyrrhotite as well as magnetite as the magnetic carriers (see Table 2, lh and lc in the rock-type column). This suggests that the host rocks, being far removed from the intrusions, were most likely not remagnetized by the volcanic intrusions but rather by a hydrothermal regime marked by Fe-oxide and pyrrhotite components.

DISPERSAL CHARACTERISTICS OF THE MAGNETIZATIONS

Geomagnetic secular variation is one of the major causes responsible for the dispersal of ancient palaeomagnetic directions. A statistic traditionally used to describe the palaeosecular variation is S_B ,

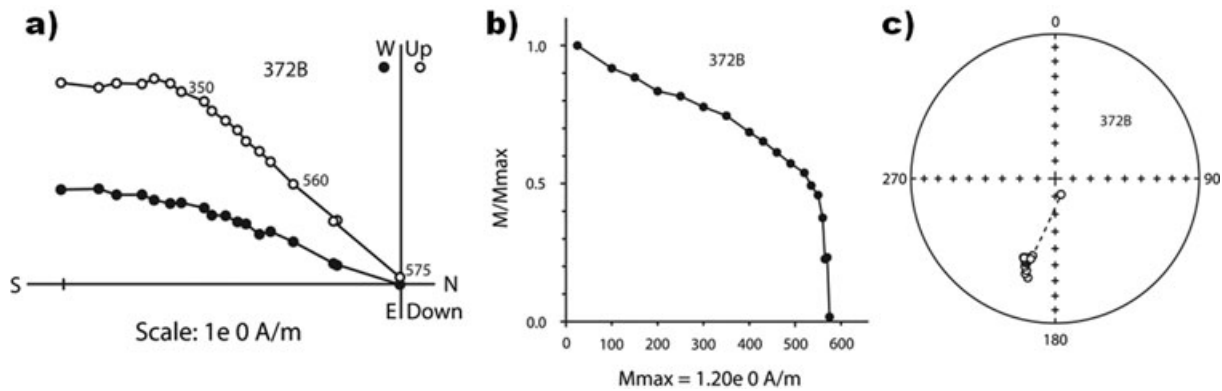


Figure 12. Thermal demagnetization of a dyke sample (#372) from site 44, in which the remanence is carried only by magnetite. The sudden drop in remanence below 350°C, diagnostic of pyrrhotite, is not present in this sample. (a) Zijderveld diagram depicting the directional trend, (b) intensity decay of sample 372 with increasing demagnetization steps (in °C), showing unblocking temperatures characteristic of low-titanium magnetite and (c) stereographic projection of the endpoint directions of sample 372 during thermal treatment up to the last (deviating) point at 575 °C, when the remanence has dwindled to less than 2 per cent.

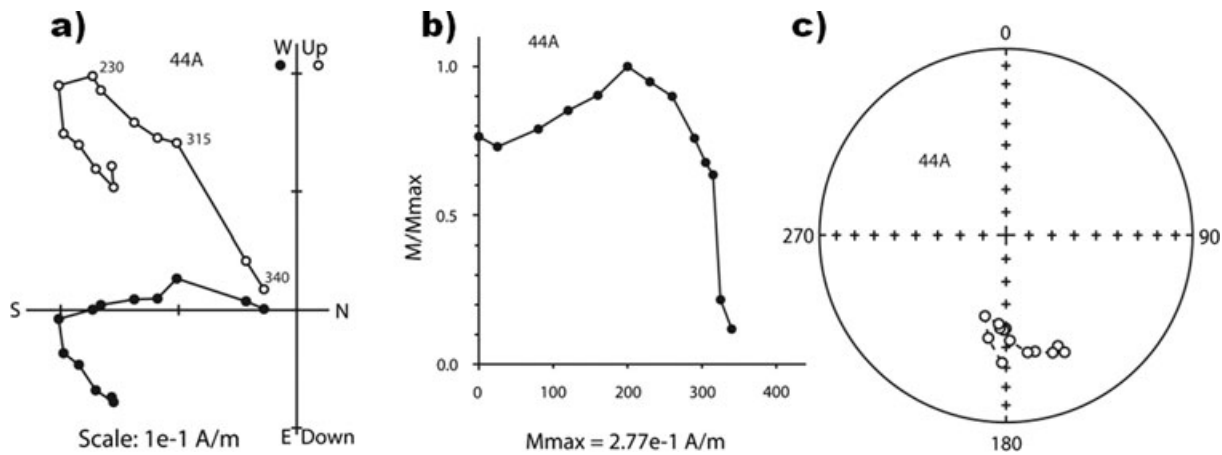


Figure 13. Thermal demagnetization of a dyke sample (#44) from site 6, with a magnetization carried by pyrrhotite only. (a) Zijderveld diagram depicting the directional trend, with a somewhat noisy behaviour, so that its MAD of 11.3° is acceptable, but well above average, (b) intensity decay of sample 44 with increasing demagnetization steps (in °C), showing unblocking temperatures characteristic of Fe-sulphide and (c) stereonet showing the vector endpoints of sample 44 as measured during thermal demagnetization.

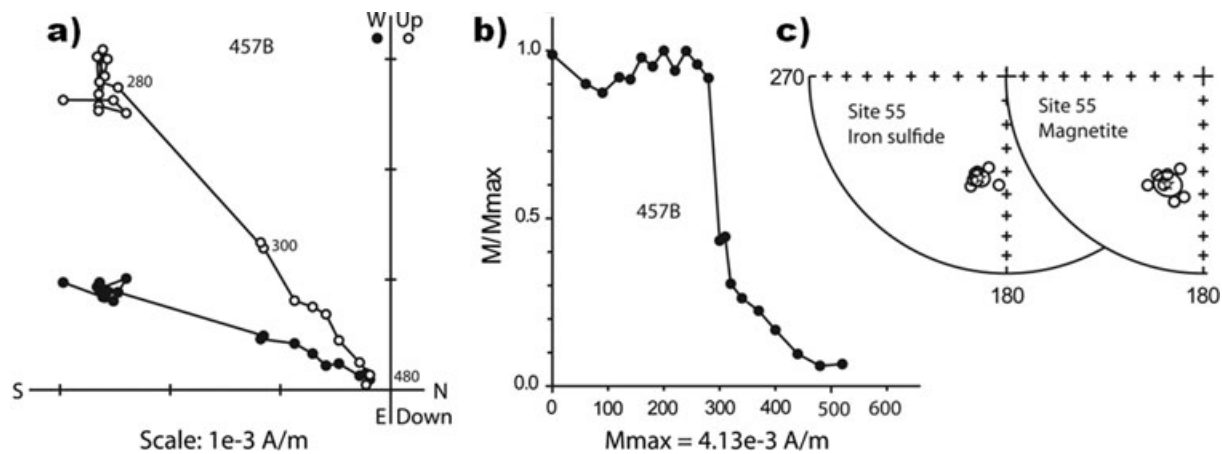


Figure 14. Thermal demagnetization of sample 457 from limestone host rock (site 55), not in the proximity of a dyke (more than 40 m away). (a) The direction for this sample is southwest and up and (b) the carriers of the magnetization appear to be an iron sulphide (with an unblocking temperature of about 300 degrees) as well as magnetite. The directions below 300 °C and those above 350° show a very slight deviation from each other. (c) The eight accepted directions for each of the Fe-sulphide and magnetite components of site 55, including sample 457.

Table 3. Overall mean palaeopoles.

Category of magnetization	Sites $\alpha_{95} > 15^\circ$	Sites, $n = 1, 2$	N	P-Lat	P-Lon	K	A_{95}	λ at Oslo
Fe-sulphides, all rock types	Included	Included	35	53.0	163.1	65.4	3.0	25.0
Fe-sulphides, all rock types	Excluded	Included	31	53.2	163.8	61.2	3.3	25.1
Fe-sulphides, all rock types	Included	Excluded	24	53.7	163.9	116.3	2.8	25.6
Fe-sulphides, all rock types	Excluded	Excluded	20	54.1	165.7	112.0	3.1	25.7
Fe-sulphides only, no magnetite	Excluded	Excluded	6	53.2	161.9	58.7	8.8	25.4
Fe-sulphides, lc only	Included	Included	6	54.8	164.2	144.5	5.6	26.6
Fe-sulphides, lh only	Included	Included	6	55.1	168.7	243.2	4.3	26.3
Fe-sulphides, lc only	Included	Excluded	4	53.7	159.4	327.6	5.1	26.3
Magnetite, all rock types	n/a	Excluded	38	51.1	162.8	88.5	2.5	23.2
Magnetite, dykes only	n/a	Excluded	25	50.9	163.8	68.7	3.5	22.9
Magnetite, lh only	n/a	n/a	6	52.4	159.8	162.5	5.3	25.0
Magnetite, lc only	n/a	Excluded	4	49.9	155.0	1066.0	2.8	23.5

Notes:

N = number of sites yielding a VGP used for the calculation. K and A_{95} are the statistical parameters associated with the mean palaeopole. lc = limestone in contact with dyke; lh = host limestone away from dyke.

P-Lat, P-Lon = latitude and longitude of the palaeopole; λ = palaeolatitude, calculated for Oslo at 60N, 10E. n/a = not applicable.

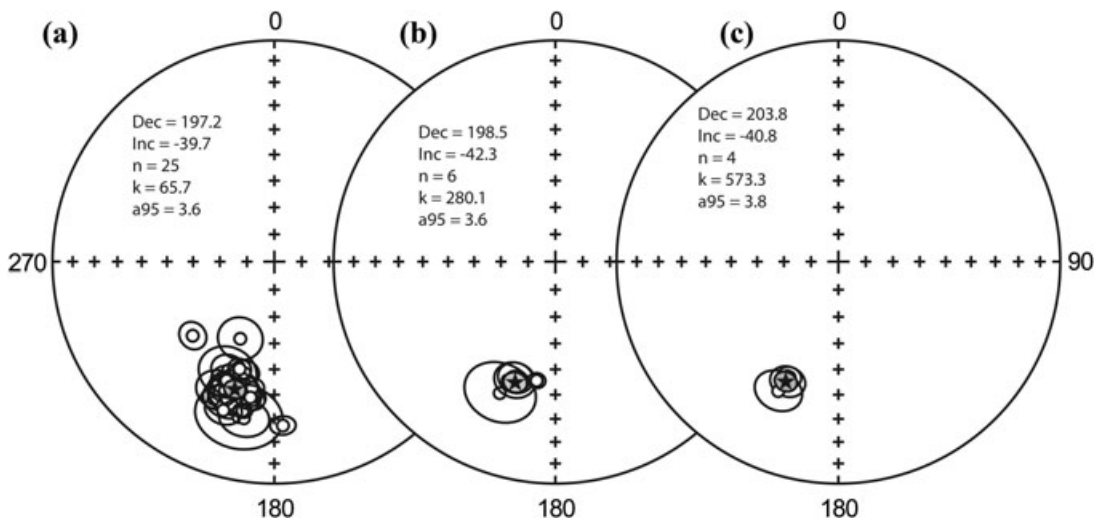


Figure 15. Stereonets showing the site-mean component directions carried by magnetite in (a) dykes, (b) contact rocks and (c) host rocks.

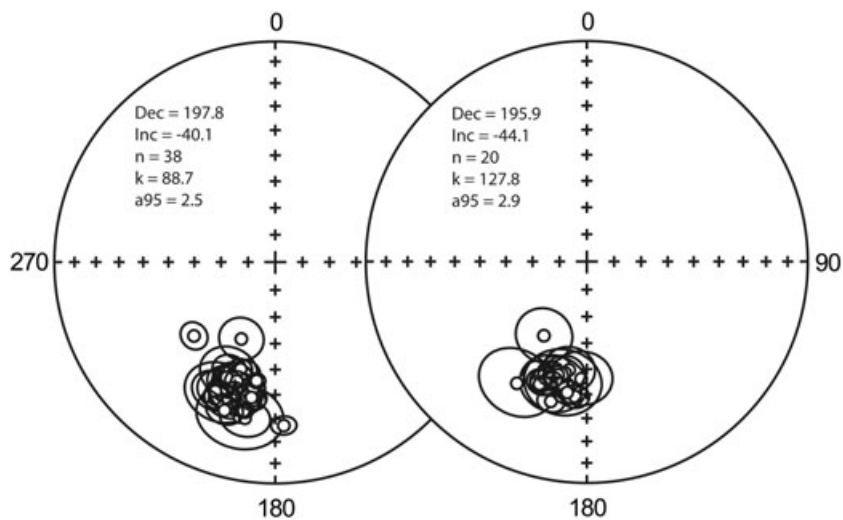


Figure 16. Stereonets showing the site-mean component directions of magnetizations carried by magnetite (left-hand side) and pyrrhotite (right-hand side), as listed in Table 2.

the rms angular deviation of the virtual geomagnetic poles (VGPs) about their mean, after correction for the dispersion due to random errors associated with sample orienting and measuring (e.g. Cox 1970; Biggin *et al.* 2008; Johnson *et al.* 2008, and references therein).

It is anticipated, but probably not yet entirely satisfactorily documented, that long intervals of one geomagnetic polarity state, such as the Kiaman Reversed Superchron or the Cretaceous Normal Superchron, have less dispersion than intervals such as the Neogene or Jurassic when reversals are frequent. What has become rather clear, however, is that clustering of VGPs that is unusually tight (say, $S_B < 7^\circ$ or $K > 90$) may reflect averaging of the geomagnetic field during long times of remanence acquisition, thereby strongly reducing the effects of secular variation. The associated low degree of dispersal, in turn, could then be taken to indicate that the associated remanence is secondary. Classical cases of remagnetization show this convincingly and frequently [an example is the remagnetized Trenton Limestone result (McCabe *et al.* 1984), which yielded $K = 98$ based on 30 site VGPs].

The multiple remanence results from the varying lithologies of our study can be interpreted with a reasonable degree of confidence as representing secondary remanences in all palaeopole determinations except one; the exception, as the only possible candidate to possess a primary remanence, is the dyke result based on magnetite components. It is therefore of interest to examine how the value of S_B associated with a given result compares with what one might expect for a primary or a secondary remanence. Table S5 contains details of the calculations, which can be summarized here by listing S_B values in parentheses for each of the magnetite remanence in the dykes (9.3°), that of the (host and contact) limestones (4.1°), and the sulphide remanence (5.6°).

Biggin *et al.* (2008) have shown that for the approximate palaeolatitude of the Oslo-Lunner dykes of about 23° and with a magnetization acquired during a superchron, one might expect an S_B value ranging between about 9 and 13° , based on both low- and high-quality data sets (their figs 7c and 8c). We note that the dispersion ($S_B = 9.3^\circ$) of our dykes' VGPs falls within this range and allows the magnetite remanence, likely acquired before the end of the Kiaman Reversed Superchron, to be interpreted as a primary remanence. In contrast, the values of S_B less than 6° , associated with the results carried by Fe-sulphides, as well as in the remagnetized host and contact limestones, are unacceptably low for a primary remanence and indicate that these results are secondary.

AGES OF THE MAGNETITE AND PYRRHOTITE REMANENCES

The more important of our two new main results is the palaeopole (51°N , 164°E ; $N = 25$ dykes, $K = 69$, $A_{95} = 3.5$; Tables 3 and 5) derived from the magnetite component in dykes only, given that it has a chance of being well dated, as we will discuss first in this section. In contrast, SEM observations of Fe-sulphides in our samples show that they are abundant and of secondary (hydrothermal) origin in all likelihood (Figs 6a and d), rendering them much less useful for tectonic analysis. The results obtained from the pyrrhotite magnetization components will be discussed after the discussion of the age of the magnetite remanence.

Age of the magnetite remanence in the dykes

We interpret the remanence carried by magnetite in the dykes as primary, that is, as having the same age as the rocks. This

interpretation follows from the following seven observations or arguments:

(1) The dykes intrude some 280 Ma rocks, implying that the remanence must be < 280 Ma.

(2) The ages determined in Torsvik *et al.* (1998) for the Lunner dykes are based on plateaus that occur next to a rising high-temperature tail-end towards older ages (more like our new ages of ~ 270 Ma). Torsvik is a co-author of both the 1998 and this study and concurs with the explanation we offer in terms of argon loss. In fact, he and his colleagues explicitly pointed out the possibility of argon loss already in the 1998 paper, and this prompted us to undertake the new age dating. The earlier age dates of 1998 must be seen as superseded.

(3) The new Ar-Ar ages of 271 ± 1.3 (1σ) Ma are more reliable than the previous ages, which showed unambiguous evidence of being influenced by some argon loss (red arrows in Fig. S1). We argue that the dykes are now well dated as 271 ± 1.3 (1σ) Ma (Cisuralian–Guadalupian boundary in the Permian).

(4) The dykes intruded in the brittle environment at shallow crustal levels and show no signs of metamorphism. A thermal resetting, producing a thermoremanent magnetization (TRM) is unlikely.

(5) Of course, the age of the magnetite magnetization could theoretically be younger than the age of the rocks, if the magnetite grew and acquired a chemical remanence (CRM) significantly after intrusion and cooling. However, the SEM images reveal that titanomagnetite occurrences show high-temperature exsolution, indicating a primary nature of these Ti-Fe oxides. It is inferred that submicrometer magnetite and the magnetite grains observed with the SEM (Fig. 6) have the same origin and history, and that no new magnetite has grown in a secondary chemical event.

(6) The dyke remanence has secular variation characteristics that agree with typical values for a primary remanence in igneous rocks at a palaeolatitude of $\sim 23^\circ\text{N}$, with $S_B = 9.3^\circ$ being quite comparable to the values in Biggin *et al.* (2008; their figs 7c and 8c) for a superchron with S_B values of about 9 – 13° . In contrast, the values of S_B for the remagnetized rocks are incompatible with a primary origin of the Fe-sulphides or the magnetites in the limestones.

(7) A new APWP segment has been constructed for Baltica for the interval of 310–230 Ma, based on an updated compilation of individual palaeopoles (Table S4). There are 85 palaeopoles of which some 21 were not yet available at the last compiling occasion some 6 yr ago (Torsvik *et al.* 2008). Reference poles are constructed with moving-windows (20 Myr durations) yielding mean poles that are 10 Myr apart (Table 4). The data set includes palaeopoles determined from clastic sediments, so the mean poles are shown in Fig. 18 without and with correction for hypothetical inclination shallowing. The purpose of these plots is to examine whether the palaeopole from the Oslo-Lunner dykes, with an age of 271 ± 1.3 (1σ) Ma, can derive agreement from Baltica's APWP. This turns out to be convincingly the case, as can be seen in the agreement between the blue-coloured cone of 95 per cent confidence (A_{95}) around the 270 Ma reference pole and the mustard-coloured A_{95} around the new Oslo-Lunner dyke magnetite pole. We also note that no significant overlap occurs between the latter and the reference poles that are either older or younger than the one at 270 Ma.

Age of the pyrrhotite remanence

Abundant Fe-sulphide grains have been observed with the SEM. However typically, the EDS spectra reveal much larger peaks for

Table 4. Running-mean south-poles for Stable Eurasia.

Age	<i>N</i>	<i>A</i> ₉₅	Plat	Plon	<i>A</i> ₉₅	Clat	Clon
230	6	5.8	-50.7	311.2	5.1	-51.8	309.7
240	8	7.1	-52.9	328.5	5.8	-56.3	325.2
250	16	3.7	-52.8	332.8	2.6	-55.6	329.8
260	20	2.8	-52.0	332.2	2.2	-54.5	329.8
270	14	3.7	-48.5	338.5	4.1	-50.9	336.6
280	27	2.4	-44.1	346.7	2.5	-44.6	346.5
290	47	1.7	-42.3	347.0	1.9	-43.1	346.5
300	27	2.3	-41.5	347.9	2.7	-42.6	347.0
310	6	6.3	-42.5	347.8	5.9	-43.5	347.0

Notes:

Individual entries are listed in the Table S4. *N* is the number of poles in the 20 Myr windows, incrementing by 10°. Plat and Plon are the coordinates of the mean poles without correction for inclination shallowing, whereas Clat and Clon are the coordinates of the mean poles after such a correction, applied only (with flattening *f* = 0.6) to results obtained from clastic sediments.

Note that this hypothetical correction succeeds in reducing many *A*₉₅ values.

S than for Fe (Fig. 6a), indicating that we are dealing with non-magnetic pyrite. From the rock and palaeomagnetic properties, we can infer that one of the two magnetic components in our samples is carried by monoclinic pyrrhotite, but we cannot be sure that the latter has the same history and appearance as the larger grained pyrite, because we have not been able to see a convincing EDS spectrum for Fe₇S₈ or something close to it. The relationship between the Fe-sulphide and Ti-Fe oxide in Fig. 6(a) suggests that the sulphide is younger, and we assume that pyrrhotite, by association, is also younger than the iron oxides.

Where both magnetite and pyrrhotite appear to contribute to the remanence in the same site-mean (Table 2), the inclination of the mean pyrrhotite magnetizations is nearly always more steeply upwards than those of the mean magnetite components (Fig. 17), with the difference averaging 3.8°. That the pyrrhotite components have steeper upward inclinations in these sites also suggests that they are

somewhat younger, given that Pangea moved steadily northwards during Late Permian–Early Triassic times.

The newly constructed APWP for Baltica for the 310–230 Ma interval (Fig. 18) has already been mentioned. The steady northward drift of Baltica causes the mean south-palaeopole for each age bin to shift from 43°S, 348°E to 51°S, 311°E. Also shown are the most representative mean poles of this study, including the pyrrhotite pole (Fig. 18c). The mean direction and palaeopole of sites that only have a pyrrhotite remanence (and no magnetite remanence, see fifth entry in Table 3) fully agrees with the means calculated in other ways.

The remanences of the accepted pyrrhotite and magnetite components are exclusively of reversed polarity. We argue, therefore, that both the magnetite and the pyrrhotite remanence were acquired near the end of the long Kiaman Reversed Superchron, that is, before 267 Ma (Gradstein *et al.* 2004; Cottrell *et al.* 2008). Given that the pyrrhotite is thought to be younger than the magnetite, the pyrrhotite remanence was most likely acquired between 274 and 267 Ma.

There is another aspect of the above-mentioned inclination comparison that deserves a brief mention and that is to note that the pyrrhotite remanence cannot be explained by proposing that it is a composite remanence, consisting of the sum of a magnetite remanence and a lower temperature present-day field component. This is graphically illustrated in Fig. S3. A composite remanence must, by definition, fall on the great circle trajectory between its constituent components—this is the illustrated case for the diagram on the left-hand side. However, the diagram on the right-hand side is the actual situation and illustrates that the steeper component falls outside this segment.

DISCUSSION

Comparing our new poles (51°N, 163°E, *N* = 38, for magnetite and 54°N, 166°E, *N* = 20, for pyrrhotite; see Table 3) with the previously published palaeopole for the Lunner dykes from the Oslo region (at 53°N, 164°E, Torsvik *et al.* 1998), one can see that these

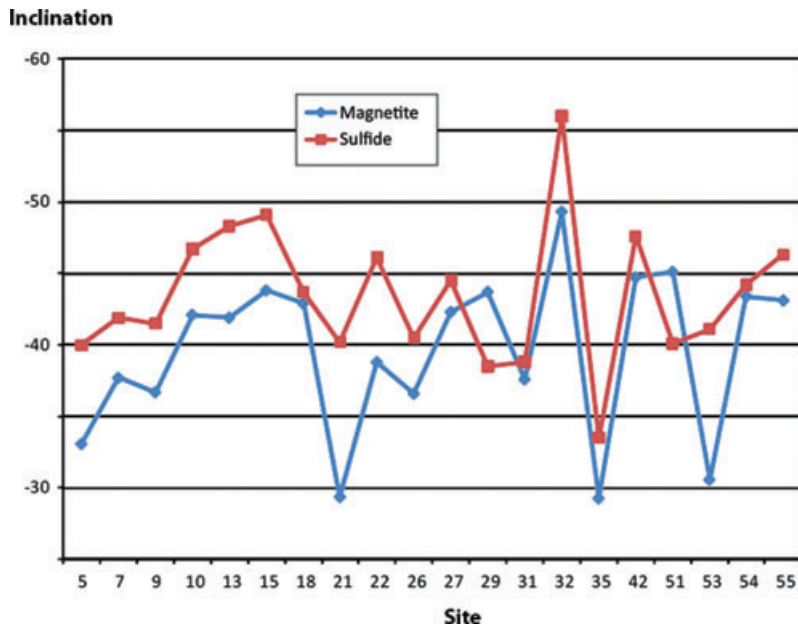


Figure 17. Plot of inclination values of the site-means calculated from pyrrhotite (red) and magnetite remanences (blue), wherever they occur together in the same sites. The inclinations are persistently more negative in the site means of the pyrrhotite components.

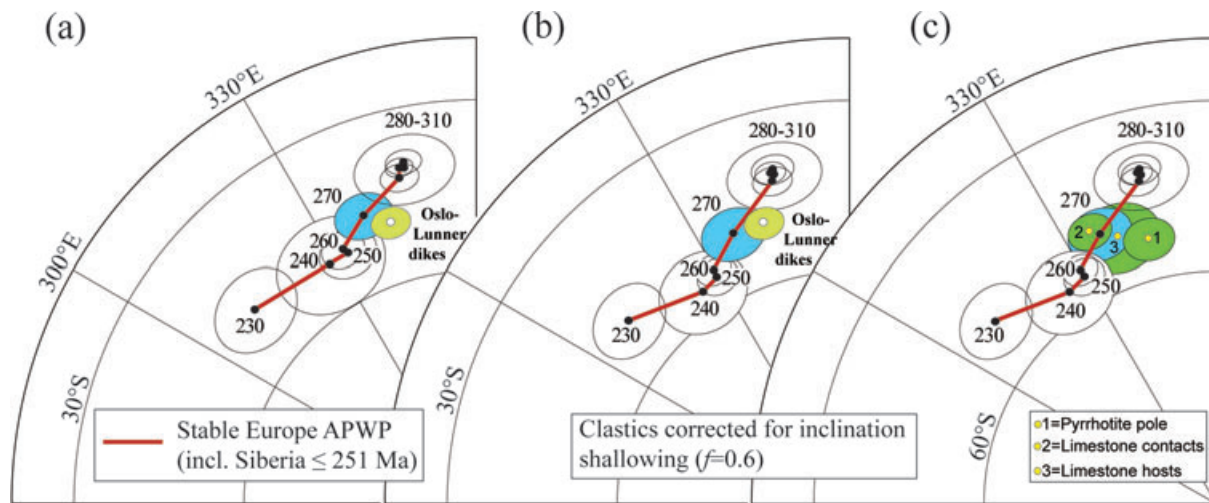


Figure 18. (a) Palaeopole from the magnetite components in Oslo-Lunner dykes only (mustard colour), together with a new APWP segment for Baltica based on palaeopoles listed in Tables 4 and S4. The A_{95} of the 270 ± 10 Ma reference pole is shaded in blue. (b) The same as (a), except that all palaeopoles based on clastic sediments have been corrected for inclination shallowing (with $f = 0.6$). (c) The same as (b), but with the palaeopoles from iron sulphide magnetic components of this study, and the poles of the magnetite residing in contact and host limestones.

palaeopoles are nearly identical, despite the much larger sampling and the separation according to magnetic carriers in this study. With the larger sampling collection, the results of this study meet several, but not all, of the seven reliability criteria of Van Der Voo (1990). Criterion 1 is met, because the $^{40}\text{Ar}/^{39}\text{Ar}$ method has given very precise ages. It is also likely that these ages (about 270 Ma) are the same as the magnetization acquisition ages for the magnetite component. Criterion 2 is met, since there are more than 25 accepted samples from the two groups of dykes and their immediate contacts, and the statistical parameters (k , α_{95}) show good precision. Criterion 3 is satisfied by the use of AF and thermal demagnetization, with the results analysed with Principal Component Analysis. Criterion 4 is not satisfied, because the contact test is inconclusive and the nature of the targeted rocks is such that no fold or conglomerate tests could be applied. Whether criterion 5 is satisfied or not, depends on the likelihood of structural tilt after dyke emplacement; in such a situation it is customary to remain conservative and let this criterion be failed. Although the Oslo Graben is clearly embedded in the cratonic part of Baltica, the possibility of late tilts of the sampling areas cannot be discounted. On the other hand, the studied dyke intrusions represent the last igneous activity in the graben, and the samples were taken over a large area (approx. 30×50 km), reducing the likelihood of a systematic bias. We should also point out that the main structural trends are approximately parallel to the mean declination of our results, which implies that unrecognized tilts of some $10\text{--}20^\circ$ would affect mostly the declinations, but hardly the inclinations. And, of course, it is the latter that establish the palaeolatitudes of the Oslo area for the Late Permian. Certainly criterion 6 is not met, as no reversals have been observed. On the other hand, our new poles do not resemble reference palaeopoles for younger periods (Fig. 18), so criterion 7 is met. Altogether this gives our result a Q -value of 4 (or perhaps 5).

The mean pole for the sites where magnetite is the main remanence carrier is slightly older than the pole based on sites with pyrrhotite remanence and this difference is statistically insignificant to marginally significant, depending on the choice of entry from Table 3. An age of 271 ± 1.3 (1σ) Ma, as determined from our new $^{40}\text{Ar}\text{--}^{39}\text{Ar}$ ages, is assigned to the magnetite remanence. The age of the sulphide remanence is more difficult to prove, but is unlikely to

be much younger than 267 Ma, judging from its pole location in Fig. 18. It could plausibly be related to a remagnetization event by hydrothermal fluids.

The controversial Pangea-B configuration has been proposed to avoid the large latitudinal overlap of $\sim 11^\circ$, which would exist between Gondwana and Laurussia if one were to keep these landmasses at approximately the same relative longitudes as they would occupy in Pangea A. The Pangea-B solution suffers from the additional complexity that Pangea B must have transformed into Pangea A before the Atlantic Ocean opened, necessitating the existence of a 3500 km dextral megashear, which must have been active either in Triassic (Irving 1977) or in mid-to-late Permian time (Muttoni *et al.* 2003). An alternative solution to the conundrum has invoked complexities in the geomagnetic field, but this has been regarded as *ad hoc* or even as unnecessary by the scientific community (see e.g. Irving 2004 for a review). Finally, flaws in the way the available magnetic directions reflect the geomagnetic field (e.g. inclination shallowing or contamination by overprints), or uncertainties in their ages have been suggested as causing, or contributing to, the problem (Rochette & Vandamme 2001; Van der Voo & Torsvik 2004; Iosifidi *et al.* 2010; Meijers *et al.* 2010). The motivation for this study was to see whether a more exhaustive study of the Lunner dykes than the one more than a decade ago (Torsvik *et al.* 1998) would contribute to a solution along the latter lines. It turns out that the palaeopole location has not changed, but instead its age has become older by nearly 30 Myr.

In Fig. 1 the palaeolatitude for Oslo is portrayed as roughly 13° N for ~ 280 Ma. Baltica moved north in the 10 Myr following (as seen in its reference palaeopoles of Fig. 18), and by 270 Ma our results indicate that Oslo reached palaeolatitudes of $23\text{--}25^\circ$ N. Table 5 lists the poles and palaeolatitudes of relevant results for the Gondwana, Laurentia and Baltica results with ages between 280 and 260 Ma, whereas Fig. 19 portrays the resulting palaeogeography for 270 ± 10 Ma. This appears to constitute sufficient improvement to lead to a solution of the Pangea problem, for mid-to-late Permian (~ 270 Ma) and younger, as it can be seen that for this time interval the Pangea A configuration is permitted. Thus the intra-Pangean megashear need not be invoked for Triassic times, as previously suggested by Irving (1977) and Torcq *et al.* (1997).

Table 5. Mean palaeopoles for Stable Europe, Laurentia & Gondwana, 260–279 Ma.

Nr.	Formation	T/DC/AQ	Palaeopole	A_{95}	Age (Ma)	Palaeolatitude and reference
Stable Europe						
1	Scania dykes, Sweden	V/3/3	54N, 172E	11	279 ± 10	$\lambda = 24.9^\circ\text{N}$ at 60N, 10E, Bylund (1974)
2	Estérel extrusives, France	V/3/2	52N, 142E	6	264–270	$\lambda = 29.5^\circ\text{N}$ at 60N, 10E, Zijdeveld (1975)
3	Cracow Volcanics B, Poland	V/4/3	50N, 164E	4.1	265–272	$\lambda = 22^\circ\text{N}$ at 60N, 10E, Nawrocki <i>et al.</i> (2008)
4	Bohuslan Dykes combined, Sweden	V/3/1	51N, 165E	8.6	250–300	$\lambda = 22.8^\circ\text{N}$ at 60N, 10E, Thorning & Abrahamsen (1980)
5	Oslo-Lunner (dykes only, magnetite)	V/4/3	51N, 164E	2.5	271 ± 2.7	$\lambda = 23^\circ\text{N}$ at 60N, 10E, this study
6	Mean of 1–4	V	51N, 161E	9.2	271 ± 8	$\lambda = 24.7^\circ\text{N}$ at 60N, 10E
7	Mean of 1–5	V	52N, 161E	6.7	271 ± 8	$\lambda = 24^\circ\text{N}$ at 60N, 10E
8	Pole from reference path (Table 4)	V+S	49N, 159E	3.7	270 ± 10	$\lambda = 22^\circ\text{N}$ at 60N, 10E, this study (no incl. correction)
9	Pole from reference path (Table 4)	V+S	51N, 157E	4.1	270 ± 10	$\lambda = 24.2^\circ\text{N}$ at 60N, 10E, this study (incl. corrected)
Laurentia						
10	Hick's Dome, Illinois	V/4/3	55N, 112E	9	268–273	Reynolds <i>et al.</i> (1997)
11	Downey's Bluff, Illinois	V/4/3	53N, 129E	4	268–273	Reynolds <i>et al.</i> (1997)
12	Mean, Illinois intrusions	V/4/3	54N, 120E		271 ± 3	$\lambda = 6^\circ\text{N}$ at 38N, 88W
Gondwana						
13	Upper Choiyoi, Argentina	V/4/3	76N, 146E	4	264 ± 4	$\lambda = 46.2^\circ\text{S}$ at 34.9S, 291.5E, Domeier <i>et al.</i> (2009)
14	Sierra Chica, Argentina	V/4/3	80N, 169E	3	263 ± 2	$\lambda = 39.7^\circ\text{S}$ at 34.9S, 291.5E, Domeier <i>et al.</i> (2011)
15	Taztot Trachyandesite, Morocco	V/2/2	39N, 237E	5	273 ± 18	Daly & Pozzi (1976)
16	Mechra-Chougrane, Morocco	V/3/2	36N, 238E	21	275 ± 18	Westphal <i>et al.</i> (1979)
17	Mean of 15 and 16	V	38N, 237E		274 ± 18	$\lambda = 1.9^\circ\text{N}$ at 32N, 353E

Notes:

T, lithology; V, volcanics; S, sedimentary rocks; DC, demagnetization code; AQ, age quality (see Van Der Voo & Torsvik 2004). λ = palaeolatitude; incl., inclination; A_{95} , radius of the cone of 95 per cent confidence about the palaeopole.



Figure 19. Baltica, Gondwana and Laurentia are positioned according to the palaeomagnetic data with ages between 260 and 280 Ma (listed in Table 5). Selected sampling localities represented by the stars and their palaeolatitude values are shown. For this Permian time interval (Cisuralian-Guadelupian epochs), a Pangea-A type fit is not creating any significant overlap of Gondwana and Laurussia.

Muttoni *et al.* (1996, 2003) advocated an earlier age (early-to-mid Permian) for the megashearing movements; with our new data from this study an Early Permian age cannot be precluded. Muttoni and colleagues also noted that the available Late Permian–Early Trias-

sic palaeomagnetic data were not of the highest quality; we certainly agree with that assessment, but hope that this and parallel studies (e.g. Domeier *et al.* 2009, 2011) will help to remedy the situation.

CONCLUSIONS

To improve upon an earlier study (Torsvik *et al.* 1998), which was rather limited in its palaeomagnetic sampling, we collected a large number (39) of Oslo-Lunner dykes. The previous dating at about 245 Ma with $^{40}\text{Ar}/^{39}\text{Ar}$ methodologies in the earlier study was marred by hints of argon loss, so new age dating with $^{40}\text{Ar}/^{39}\text{Ar}$ was also carried out, and yielded somewhat older ages of $271 \pm 1.3 (1\sigma)$ Ma, without complexities such as argon loss. 25 of the dykes yielded magnetization directions carried by low-Ti magnetite. Limestone sites in contact with the dykes as well as limestone sites away from the thermal effects of the intrusions carry a similar magnetization. We also observed magnetizations with the characteristics of pyrrhotite as their carrier in some 35 sites of dykes and limestones. The baked contact tests, for which the limestone and a few igneous host rock sites were specifically collected, are inconclusive.

We infer from SEM observations that the pyrrhotite magnetization is secondary and is slightly younger than the magnetite magnetization. It is likely that the sulphides formed as a result of hydrothermal circulation during the waning stages of the faulting and igneous activity of the Oslo Graben.

We find that Oslo was at a palaeolatitude of about $22\text{--}25^\circ\text{N}$, in agreement with predicted palaeolatitudes from the Scania dykes (Bylund 1974) and the Cracow Volcanics B pole (Nawrocki *et al.* 2008), which are the only other volcanic and well-dated results for 270 ± 10 Ma for Baltica (Table 5). A mean reference palaeopole from a newly compiled Baltica palaeopole database also predicts such a palaeolatitude. Our new result substantiates the Pangea-A type palaeogeography for this time, as it leaves enough room between Laurentia, Baltica and Gondwana, thereby eliminating the overlap between the Laurussia and Gondwana continental masses for Late Permian and younger times. A similar conclusion was reached by Muttoni *et al.* (1996, 2003) for ~ 280 Ma, whereas a new palaeopole that has recently become available from Ukraine dykes (~ 282 Ma, Yuan *et al.* 2011; see also Iosifidi *et al.* 2010; Meijers *et al.* 2010) and two new Late Permian palaeopoles at 80.1°S , 349°E and 76°S , 326°E from Argentinian volcanics (263 ± 2 Ma and 264 ± 4 Ma, Domeier *et al.* 2009, 2011) also confirm this conclusion. It remains permitted to place the Pangea B to Pangea A transformation in earlier Permian or Carboniferous time, of course. Better determined palaeopoles from the West Gondwana continents are needed to refine the conclusions about any continental overlap during the earlier Permian.

ACKNOWLEDGMENTS

We warmly express our gratitude to Michel Heeremans for his contribution to our general understanding of the geology of the Oslo Graben. His thorough explanation of its formation (especially in <http://www.mantleplumes.org/Norway.html>) was crucial to us in our efforts to acquire a more in-depth knowledge of the geological history of the region and as a complement to the background understanding of the region. We would also like to thank Stephen Crabtree for his assistance in the collection of the samples in the field in Norway, Fatim Hankard for helping with Palaeomac and Adobe Illustrator software, Michael Jackson for guidance with the use of the IRM equipment, Anja Schleicher and Devon Renock for their help with the SEM and EDS analysis, Carl Henderson for his help with the use of the microprobe, Stephen Kesler with identification of minerals under the optical microscope and with the SEM and Pavel Doubrovine for help with his program to calculate dispersion parameters. The journal's reviewers and Editor A. J.

Biggin are thanked for their suggestions to improve the manuscript. Partial financial support for this research was provided by the Norwegian Geological Survey (NGU) and the U.S. National Science Foundation, Division of Earth Sciences (Tectonics Program) and NSF's Office of International Science and Engineering (Americas Program), grant EAR-0634807, and is gratefully acknowledged.

Authors' contributions ARD carried out most of the palaeomagnetic and electron microbeam laboratory work and wrote an undergraduate Honors Thesis about the results reported herein. RVdV participated in the fieldwork, supervised the students working on the project, was coresponsible for the financial arrangements and contributed significant parts of this manuscript. THT participated in the fieldwork, was coresponsible for the financial arrangements and arranged for the use of NGU's $^{40}\text{Ar}/^{39}\text{Ar}$ facility. BWHH carried out the $^{40}\text{Ar}/^{39}\text{Ar}$ age dating in the laboratory in Trondheim and contributed its interpretation. AA carried out a significant part of the palaeomagnetic laboratory measurements, whereas MD was responsible for the rock magnetic characterization of the collection. BTL hosted us in the field, showing many of the important locations where sampling could be carried out and provided much insight into the geological setting of the Oslo Graben. SR participated in the fieldwork, and carried out sampling for the radiometric age dating. All coauthors have reviewed the manuscript before submission.

REFERENCES

- Biggin, A.J., Van Hinsbergen, D.J.J., Langereis, C.G., Straathof, G.B. & Deenen, M.H.L., 2008. Geomagnetic secular variation in the Cretaceous Normal Superchron and in the Jurassic, *Phys. Earth planet. Int.*, **169**, 3–19.
- Brekke, H., Sjulstad, H.I., Magnus, C. & Williams, R.W., 2001. Sedimentary environments offshore Norway: an overview, *Norwegian Petrol. Soc. Spec. Pub.*, **10**, 7–37.
- Briden, J.C., Smith, A.G. & Sallomy, J.T., 1971. The geomagnetic field in Permo-Triassic time, *Geophys. J. R. astr. Soc.*, **23**, 101–117.
- Bullard, E.C., Everett, J.E. & Smith, A.G., 1965. The fit of the continents around the Atlantic, *Phil. Trans. R. Soc. London, Ser. A.*, **258**, 41–51.
- Bylund, G., 1974. Paleomagnetism of dykes along the southern margin of the Baltic Shield, *Föreningens I Stockholm Forhandl.*, **96**, 231–235.
- Cocks, L.R.M. & Worsley, D., 1993. Late Llandovery and early Wenlock stratigraphy and ecology in the Oslo Region, Norway, *Bull. Nat. Hist. Museum (Geology)*, **49**, 31–46.
- Cogné, J.P., 2003. PaleoMac: a Macintosh (TM) application for treating paleomagnetic data and making plate reconstructions, *Geochem. Geophys. Geosyst.*, **4**, 1–8.
- Cottrell, R.D., Tarduno, J.A. & Roberts, J., 2008. The Kiama reversed polarity superchron at Kiama: toward a field strength estimate based on single silicate crystals, *Phys. Earth planet. Int.*, **169**, 49–58.
- Cox, A., 1970. Latitudinal dependence of the angular dispersion of the geomagnetic field, *Geophys. J. R. astr. Soc.*, **20**, 253–269.
- Dahlgren, S. & Corfu, F., 2001. Northward sediment transport from the late Carboniferous Variscan Mountains: Zircon evidence from the Oslo Rift, Norway, *J. Geol. Soc. London*, **158**, 29–36.
- Dalrymple, G.B., Alexander, E.C., Lanphere, M.A. & Kraker, G.P., 1981. Irradiation of samples for $^{40}\text{Ar}/^{39}\text{Ar}$ dating using the Geological Survey TRIGA reactor, *Geol. Surv. Professional Paper* 1176, 1–55.
- Daly, L. & Pozzi, J. P., 1976. Résultats paléomagnétiques du Permien inférieur et du Trias Marocain: comparaison avec les données africaines et sud-américaines, *Earth planet. Sci. Lett.*, **29**, 71–80.
- Dekkers, M.J., Mattei, J.-L., Fillion, G. & Rochette, P., 1989. Grain-size dependence of the magnetic behavior of pyrrhotite during its low-temperature transition at 34 K, *Geophys. Res. Lett.*, **16**, 855–858.
- Domeier, M., Van Der Voo, R., Tomezzoli, R.N., Torsvik, T.H., Vizan, H., Dominguez, A. & Kirshner, J., 2009. Alternative Pangea reconstructions: a matter of flawed data? Implications of a new Early Triassic

- Paleopole from Argentina, *AGU Program and Abstracts*, Abstract GP11A-05.
- Domeier, M., Van Der Voo, R., Tohver, E., Tomezzoli, R.N., Vizan, H., Torsvik, T.H. & Kirshner, J., 2011. A New Late Permian Constraint on the Apparent Polar Wander Path of Gondwana, *Geochem. Geophys. Geosyst.*, in press.
- Eide, E.A., Osmundsen, P.T., Meyer, G.B., Kendrick, M.A. & Corfu, F., 2002. The Nesna Shear Zone, north-central Norway: an $^{40}\text{Ar}/^{39}\text{Ar}$ record of Early Devonian–Early Carboniferous ductile extension and unroofing, *Norwegian J. Geol.*, **82**, 317–339.
- Gradstein, F.M., Ogg, J.G. & Smith, A.G., 2004. *A Geologic Time Scale 2004*, Cambridge University Press, Cambridge, 610 pp.
- Hallam, A., 1983. Supposed Permo-Triassic megashear between Laurasia and Gondwana, *Nature*, **301**, 499–502.
- Heeremans, M., 2005. A plume beneath the Oslo Graben? Available at <http://www.mantleplumes.org/Norway.html> (last accessed 2009 May 20).
- Henningsmoen, G., 1978. Sedimentary rocks associated with the Oslo region lavas, in *The Oslo Paleorift: A Review and Guide to Excursion*, Vol 45(7), pp. 17–24, eds Dons, J.A. & Larsen, B.T., Bull. Norges Geol. Undersøk.,
- Housen, B.A., Banerjee, S.K. & Moskowitz, B.M., 1996. Low-temperature magnetic properties of siderite and magnetite in marine sediments, *Geophys. Res. Lett.*, **23**, 2843–2846.
- Iosifidi, A. G., Mac Niocaill, C., Khramov, A. N., Dekkers, M. J. & Popov, V. V., 2010. Palaeogeographic implications of differential inclination shallowing in Permo-carboniferous sediments from the Donets Basin, Ukraine, *Tectonophysics*, **490**, 229–240.
- Irving, E., 1967. Paleomagnetic evidence for shear in the Tethys, in *Aspects of Tethyan biogeography*, Vol 7, pp. 59–76, eds Adams, C.G. & Ager, D.V., Systematics Assoc. Publ., London.
- Irving, E., 1977. Drift of the major continental blocks since the Devonian, *Nature*, **270**, 304–309.
- Irving, E., 2004. The Case for Pangea B, and the Intra-Pangean Megashear, *Geophys. Monogr.*, **145**, 13–27.
- Johnson, C.L. et al. 2008. Recent investigations of the 0–5 Ma geomagnetic field recorded by lava flows, *Geochemist. Geophys. Geosyst.*, **9**, Q04032, doi:10.1029/2007GC001696.
- Kirschvink, J.L., 1980. The least squares line and plane and the analysis of paleomagnetic data, *Geophys. J. R. astr. Soc.*, **62**, 699–718.
- Larsen, B.T., Olausson, S., Sundvoll, B. & Heeremans, M., 2008. The Permo-Carboniferous Oslo Rift through six stages and 65 million years, *Episodes*, **31**, 52–58.
- Lowrie, W., 1994. Identification of ferromagnetic minerals in a rock by coercivity and unblocking temperature properties, *Geophys. Res. Lett.*, **17**, 159–162.
- McCabe, C., Van Der Voo, R. & Ballard, M. M., 1984. Late paleozoic remagnetization of the Trenton Limestone, *Geophys. Res. Lett.*, **11**, 979–982.
- McDougall, I. & Harrison, T.M., 1999. *Geochronology and Thermochronology by the $^{40}\text{Ar}/^{39}\text{Ar}$ method*. Oxford Monographs on Geology and Geophysics no. 9, 2nd edn, Oxford University Press, New York, NY, 269 pp.
- Meijers, M., Hamers, M.F., van Hinsbergen, D., Van Der Meer, D., Kitchka, A., Langereis, C. & Stephenson, R., 2010. New late Paleozoic paleopoles from the Donbas Foldbelt (Ukraine): implications for the Pangea A vs. B controversy, *Earth planet. Sci. Lett.*, **297**, 18–33.
- Mosar, J., Torsvik, T.H. & BAT team, 2002. Opening of the Norwegian and Greenland Seas: Plate tectonics in Mid Norway since the Late Permian, *Geological Survey of Norway*, pp. 48–59.
- Muttoni, G., Kent, D.V. & Channell, J. E. T., 1996. Evolution of Pangea: paleomagnetic constraints from the Southern Alps, Italy, *Earth planet. Sci. Lett.*, **140**, 97–112.
- Muttoni, G., Kent, D.V., Garzanti, E., Bracke, P., Abrahamsen, N. & Gaetani, M., 2003. Early Permian Pangea ‘B’ to Late Permian Pangea ‘A’, *Earth planet. Sci. Lett.*, **215**, 379–394.
- Nawrocki, J., Fanning, M., Lewandowska, A., Polechońska, O. & Werner, T., 2008. Palaeomagnetism and the age of the Cracow volcanic rocks (S Poland), *Geophys. J. Int.*, **174**, 475–488.
- Olausson, S., 1981. Marine incursion in upper Paleozoic sedimentary-rocks of the Oslo Region, Southern-Norway, *Geol. Mag.*, **118**, 281–288.
- Olausson, S., Larsen, B.T. & Steel, R., 1994. The Upper Carboniferous–Permian Oslo Rift; basin fill in relation to tectonic development, *Canadian Soc. Petrol. Geol. Mem.*, **17**, 175–197.
- Ramberg, I.B. & Larsen, B.T., 1978. Tectonomagmatic evolution, eds Dons, J.A. & Larsen, B.T. The Oslo Paleorift: a review and guide to excursions, *Bull. Norges Geol. Undersøk.*, **337**, 55–73.
- Rex, D. C. & Guise, P. G., 1995. Evaluation of argon standards with special emphasis on time scale measurements, *Bull. Lias. Inform. IUGS Subcom. Geochronol.*, **13**, 21–23.
- Reynolds, R.L., Goldhaber, M. B. & Snee, L. W., 1997. Paleomagnetic and $^{40}\text{Ar}/^{39}\text{Ar}$ results from the Grant intrusive breccia and comparison to the Permian Downeys Bluff Sill: evidence for Permian igneous activity at Hicks Dome, southern Illinois Basin, *USGS Bull.*, 2094-G.
- Roberts, A.P., Pike, C.R. & Verosub, K.L., 2000. First-order reversal curve diagrams: a new tool for characterizing the magnetic properties of natural samples, *J. geophys. Res.*, **105**, 28 461–28 475.
- Rochette, P. & Vandamme, D., 2001. Pangea B: an artifact of incorrect paleomagnetic assumptions? *Annali Geofis.*, **44**, 649–58.
- Rochette, P., Fillion, G., Mattéi, J.L. & Dekkers, M.J., 1990. Magnetic transition at 30–34 Kelvin in pyrrhotite: insight into a widespread occurrence of this mineral in rocks, *Earth planet. Sci. Lett.*, **98**, 319–328.
- Smith, A.G. & Livermore, R.A., 1991. Pangea in Permian to Jurassic times, *Tectonophysics*, **187**, 135–179.
- Sundvoll, B. & Larsen, B.T., 1993. Rb-Sr and Sm-Nd relationship in dyke and sill intrusions in the Oslo Rift and related areas, *Bull. Norges Geol. Undersøk.*, **425**, 25–42.
- Sundvoll, B., Neumann, E.R., Larsen, B.T. & Tuen, E., 1990. Age relations among Oslo Rift magmatic rocks: implications for tectonic and magmatic modeling, *Tectonophysics*, **178**, 67–87.
- Sundvoll, B., Larsen, B.T. & Wandaas, B., 1992. Early magmatic phase in the Oslo Rift and its related stress regime, *Tectonophysics*, **208**, 37–54.
- Thorning, L. & Abrahamsen, N., 1980. Palaeomagnetism of Permian multiple intrusion dikes in Bohuslän, SW Sweden, *Geophys. J. R. astr. Soc.*, **60**, 163–185.
- Timmerman, M.J., Heeremans, M., Kirstein, L.A., Larsen, B.T., Spencer-Dunworth E.A. & Sundvoll, B., 2009. Linking changes in tectonic style with magmatism in northern Europe during the late Carboniferous to latest Permian, *Tectonophysics*, **473**, 375–390.
- Torqu, F., Besse, J., Vaslet, D., Marcoux, J., Ricou, L.E., Halawani, M. & Basahel, M., 1997. Paleomagnetic results from Saudi Arabia and the Permo-Triassic Pangea configuration, *Earth planet. Sci. Lett.*, **148**, 553–567.
- Torsvik, T. H. & Cocks, L.R.M., 2004. Earth geography from 400 to 250 Ma: a palaeomagnetic, faunal and facies review, *J. geol. Soc. Lond.*, **161**, 555–572.
- Torsvik, T.H. & Cocks, L.R.M., 2005. Norway in space and time: a Centennial Cavalcade, *Norwegian J. Geol.*, **85**, 73–86.
- Torsvik, T.H., Eide, E.A., Meert, J.G., Smethurst, M.A. & Walderhaug, H.J., 1998. The Oslo Rift: new palaeomagnetic and $^{40}\text{Ar}/^{39}\text{Ar}$ age constraints, *Geophys. J. Int.*, **135**, 1045–1059.
- Torsvik, T.H., Briden, J. C. & Smethurst, M.A., 2000. Available at: <http://www.geodynamics.no/software.htm>. (last accessed 2010 April 2)
- Torsvik T.H., Muller R.D., Van Der Voo R., Steinberger B. & Gaina C., 2008. Global plate motion frames: toward a unified model, *Rev. Geophys.*, **46**, 1–44.
- Van Der Voo, R., 1990. The reliability of paleomagnetic data, *Tectonophysics*, **184**, 1–9.
- Van Der Voo, R. & French, R.B., 1974. Apparent polar wander for the Atlantic-bordering continents: late Carboniferous to Eocene, *Earth Sci. Rev.*, **10**, 99–119.
- Van Der Voo, R. & Torsvik, T.H., 2001. Evidence for late Paleozoic and Mesozoic non-dipole fields provides an explanation for the Pangea reconstruction problems, *Earth planet. Sci. Lett.*, **187**, 71–81.
- Van Der Voo, R. & Torsvik, T.H., 2004. The quality of European Permo-Triassic paleopoles and its impact on Pangea Reconstructions, *Geophys. Monogr.*, **145**, 29–42.
- Van Der Voo, R., Peinado, J. & Scotese, C.R., 1984. A paleomagnetic reevaluation of Pangea reconstructions, *Geodyn. Ser.*, **12**, 11–26.

- Weil, A. B., Van Der Voo, R. & Van Der Pluijm, B. A., 2001. Oroclinal bending and evidence against the Pangea megashear: the Cantabria-Asturias Arc (northern Spain), *Geology*, **29**, 991–994.
- Westphal, M., Montigny, R., Thuizat, R., Bardou, C., Bossert, A., Hamzeh, R. & Rolley, J. P., 1979. Paléomagnétisme et datation du volcanisme permien, triassique et crétacé du Maroc, *Can. J. Earth Sci.*, **16**, 2150–2164.
- Yuan, K., Van Der Voo, R., Bazhenov, M.L., Bakhmutov, V., Alekhin, V. & Hendriks, B.W.H., 2011. Permian and Triassic paleolatitudes of Ukrainian Shield with implications for Pangaea Reconstructions, *Geophys. J. Int.*, **184**, 595–610.
- Zijderveld, J.D.A., 1967. A.C. demagnetization of rocks, in *Methods in Palaeomagnetism*, pp. 256–286, eds Collinson, D.W., Creer, K.M., Runcorn, S.K., Elsevier, New York, NY.
- Zijderveld, J.D.A., 1975. Paleomagnetism of the Estérel rocks, *Ph.D. thesis*. Univ. Utrecht, 199 pp.
- Zijderveld, J.D.A., Hazeu, G.J.A., Nardin, M. & Van Der Voo, R., 1970. Shear in the Tethys and the Permian paleomagnetism of the southern Alps including new results, *Tectonophysics*, **10**, 639–661.

SUPPORTING INFORMATION

Additional Supporting Information may be found in the online version of this article:

Figure S1. $^{40}\text{Ar}/^{39}\text{Ar}$ age dating diagrams of Torsvik *et al.* (1998), showing their choices of the steps that define plateaus. They noted for sample LU1 (see ‘note’) that higher temperature steps are associated with older ages (more like 265 Ma). The red arrows show these trends for all three diagrams, suggesting that these samples suffered argon loss.

Figure S2. Examples of rejected component directions. (a) A low unblocking temperature remanence (northerly and downwards)

most likely overlaps significantly with the magnetite component above 510 °C. (b) The decay of the remanence as $f(T)$ of the same sample as in (a). (c) Shows the great-circle trajectory corresponding to the removal of the overprint. (d) Shows the 75 component directions that have been rejected as ‘anomalous’ (see Tables S1 and S2), and (e) and (f) show two examples of thermal demagnetizations where components residing in pyrrhotite (sample 361b) and magnetite (sample 10b) have MAD angles greater than 15°.

Figure S3. Schematic vertical-plane-only demagnetization diagram, illustrating the effect of a viscous or recent chemical remanent magnetization, overprinting a magnetite remanence (red) on the left, causing the blue trajectory to appear as a separate component, whereas in reality it is a composite ‘pseudocomponent’. Such a component would have a direction that falls between those of the overprint and the magnetite. In contrast, the observation that the intermediate component on the right-hand side (orange) is steeper than the magnetite component, implies that the intermediate component is not a composite, and instead is real. The latter situation is observed in this study, where the orange component is carried by pyrrhotite.

Tables S1 and S2. Specimen characteristic directions.

Table S3. Complete ^{40}Ar – ^{39}Ar data.

Table S4. Palaeopoles for Stable Eurasia (Baltica, plus Siberia after 260 Ma).

Table S5. Calculation of angular dispersion of VGPs.

Please note: Wiley-Blackwell are not responsible for the content or functionality of any supporting materials supplied by the authors. Any queries (other than missing material) should be directed to the corresponding author for the article.